Model updating of a historic concrete bridge by sensitivity- and global optimization-based Latin Hypercube Sampling

Rosalba FERRARI, Diego FROIO, Egidio RIZZI*
University of Bergamo, Department of Engineering and Applied Sciences
viale G. Marconi 5, I-24044 Dalmine (BG), Italy

Carmelo GENTILE
Politecnico di Milano, Department of Architecture, Built environment and Construction engineering (DABC)
via G. Ponzio, 31, I-20133 Milano, Italy

Eleni N. CHATZI
Institute of Structural Engineering, Department of Civil, Environmental and Geomatic Engineering, ETH Zürich,
Stefano-Franscini-Platz 5, CH-8093 Zürich, Switzerland

*Corresponding Author, email: egidio.rizzi@unibg.it

Submitted: April 14, 2017; Revised: December 22, 2017; Re-Revised: June 25, 2018

Abstract

In this paper, a self-implemented model updating global optimization procedure is successfully applied to a remarkable case study concerning a historic centennial Reinforced Concrete (RC) bridge with parabolic arches, based on recorded experimental vibrational data and arising identification of modal properties. In order to boost the degree of confidence and robustness of the developed model updating procedure, appropriate computational strategies are proposed at the level of both Sensitivity Analysis (SA) and global optimization. In particular, Latin Hypercube Sampling (LHS) is employed in drawing up both strategies, as a systematic automated way to determine appropriate multi-start sets of initiation points, optimally distributed throughout the parametric domain. The procedure involves a gradient-based method and proposes an interaction algorithm between mechanical FEM solver and numerical computing environment. Moreover, the gradient of the objective function involved in the model updating is analytically derived, instead of by often-used Finite Differences (FD), toward better accuracy and computational efficiency. Comprehensive updating results starting from a first FEM base model are achieved, for the considered case study, and show that the relative eigenfrequency and mode shape estimations are considerably improved, for all the structural modes accounted for within the updating process, with a very good final matching between experimentally extracted and FEM modelled modal properties.

***Keywords**: Structural identification; Model updating; Latin Hypercube Sampling (LHS); Sensitivity Analysis (SA); Global optimization; Historic Centennial Reinforced Concrete (RC) arch bridge.*

1 Introduction

The combination of in-situ testing and computer modeling represents a crucial means for the Structural Health Monitoring assessment of existing civil engineering structures. Such a combination relies on the so-called *model updating*, also referred to as *model calibration* (e.g. Ribeiro et al. [1], Shabbir and Omenzetter [2], Bedon et al. [3]). This process typically includes the following sequence: to acquire – to model – to update the model. It consists of a complex procedure in which each link of the chain constitutes a rather non-straightforward operation. It refers to situations in which one seeks to combine information from testing activities and analytical or numerical (typically FEM) models of the as-build structure, in order to achieve a realistic representation of the targeted construction. Specifically, a reconciling process between experimental evidence and model response is attempted.

Within the dynamic range of structural response, natural frequencies and mode shapes may be considered as well-suited characteristics toward FEM model updating purposes. In fact, they provide detailed information regarding the global and local behaviors of a structure, in terms of mass and stiffness distribution, and may be identified from acquired data during vibrational recordings, even along operational states of the structure (by Operational Modal Analysis (OMA) approaches). In this case, the above-mentioned sequence for model updating becomes: to acquire – to identify – to model – to update the model. To identify modal properties of a structure constitutes by itself a non-trivial operation, and particular efforts are commonly devoted to handle just such a task. For an extensive review on OMA approaches and related system identification methods, the reader may e.g. be referred to the work by Reynders [4]; the contributions by Mottershead and Friswell [5,6] and Fritzen et al. [7] also represent standard references on vibration-based model updating. Recent contributions to OMA approaches may additionally be found in the works by Benedettini and Gentile [8], Ubertini et al. [9], Pioldi et al. [10–12], Cardoso et al. [13], and references quoted therein.

This paper pertains to a comprehensive model updating case study concerning a hundred-year old RC bridge with parabolic arches (1917) located in Brivio, northern Italy, over the Adda river, between the provinces of Lecco and Bergamo. Thereby, the modal identification phase becomes part of the updating procedure, after an experimental campaign that was earlier carried out (2014) by ambient vibrational measurements. In particular, the paper focuses on the calibration phase of a 3D FEM model of the structure, based on the modal properties that are acquired by prior OMA processing of the recorded experimentation data. It follows in continuity with previous works on this specific subject, in which preliminary studies were conducted on the identification of the modal properties of the bridge (see Ferrari et al. [14, 15], also based on Heterogeneous Data Fusion, as additionally explored in Ravizza et al. [16]) and on the associated modelization phase (see Ferrari et al. [17]). Specifically, the paper develops a fully automated and consistent FEM updating approach, in which the matching process between experimental evidence and model response is governed by an enhanced Sensitivity Analysis-based (SA-based) and global optimization-based algorithm.

It is worth to note that so far the paper considers a fully deterministic approach, toward the model updating purposes. In this sense, other valuable model updating approaches accounting for uncertainty, e.g. based on Bayesian parameter estimation methods (see e.g. Beck and Katafygiotis [18], as a first introduction on the principle of Bayesian parameter estimation and Behmanesh et al. [19], as a recent reformulation of such a principle for structural identification) are not considered within the present discussion.

SA-based algorithms belong to the realm of optimization procedures and they are very common in structural engineering. For example, based on SA, Bakir et al. [20] propose the use of a constrained optimization algorithm for damage detection purposes, with particular reference to the analysis of buildings. In Jaishi and Ren [21], the FEM model of a concrete-filled steel tubular arch bridge is updated; in a later work by Jaishi and Ren [22], a SA-based FEM model updating is carried out for the damage detection in a RC beam. Lu et al. [23] combine SA with a two-level neural network, to improve the FEM model updating procedure, and a numerical case study is engaged to verify the proposed algorithm. In Moaveni et al. [24], a SA-based FEM model updating method is combined with an uncertainty analysis, to update the FEM model of a seven-story RC wall building structure.

More recently, Nguyen et al. [25] have assessed the serviceability limit state of vibrations of a high-performance fiber RC bridge, using vehicle-bridge interaction within the model updating procedure; in Polanco et al. [26], the use of SA-based model updating is employed to determine the degree of composite behavior of the operational bridge decks, with uncertain shear connectors.

As far as complex structures are concerned, such as combined cable-stayed suspension bridges, SA-based model updating methods may be combined with the introduction of sub-structuring, in order to improve the computational efficiency of the model updating process (Friswell and Mottershead [5]). A substructuring FEM updating method is discussed in detail by Weng et al. [27], from the SA point of view. An example of this operating way is provided by Jang and Smyth [28], in which an optimization procedure dealing with nonlinear inequality constraints is employed for the FEM model updating of a bridge; also, combining the substructure-based model updating method with the Response Surface (RS) method, a cable-stayed suspension model bridge is updated by Shan et al. [29]. However, RS-based FEM model updating relies on the so-called Variance Analysis-based (VA-based) algorithms (Catbas et al. [30], Guillaume et al. [31]), which are founded, unlike SA-based methods, on the statistical analysis of the uncertainties linked to the structure and the measured data.

A major advantage of resorting to optimization routines is that the updating procedure becomes automated, thus abandoning typical empirical processes of "manual tuning", despite for the possible drawback that the tuning problem may become intrinsically ill-posed. This commonly occurs when several uncertainties may be linked to the structure of interest, in particular with regard to material properties, geometrical features and boundary conditions. This may mathematically translate into the existence of multiple local minima of the optimization problem, instead as of a single global one. In such cases, appropriate strategies should necessarily be provided. In fact, if a local minimum is mistaken for a global one, a wrong updating solution may eventually be provided.

To avoid local minima, multi-start optimization methods began to be widely used in the 1980s (see for instance Boender and Rinnooy Kan [32]). Moreover, at the beginning of 2000, some other advanced improvements were proposed, in accordance to multi-start optimization strategies, such as, for example, criteria relating to couple local search points, to obtain a unique solution (see for instance Suykens et al. [33]). Moreover, a certain amount of research effort in that context has been devoted to improve evolutionary and genetic algorithms toward global optimization, by the so-called surrogate-assisted evolutionary algorithm (see for instance Jin [34], Müller et al. [35], Vincenzi and Savoia [36]).

In this paper, a compact SA- and global optimization-based model updating strategy, belonging to the realm of multi-start optimization methods, is proposed to avoid possibly falling on local minima, toward the model updating of a challenging case study based on real experimental modal properties. It consists in first seeking several optimization paths that take off from different *initiation points* (or *initial guess points* or *start points*); then, in analyzing the set of the obtained solutions leading to potentially different optima; finally, in selecting the global optimum among them. The procedure involves a Trust Region (TR) algorithm (Nocedal and Wright [37]) as a local searching method. It is conceived as a gradient-based method (convex programming), able to find the optima in the basins of attraction of the considered initiation point. The procedure is based on the evidence that the closer to the authentic optimum solution one may place the initiation point, the higher is the recorded probability not to fall on a local minimum. Having more than one initiation point, the probability of an initiation point to be closer to the proper solution (global optimum) increases as well. Furthermore, in order to make the procedure self-consistent, the efficient Latin Hypercube Sampling (LHS) method (McKay et al. [38]) is systematically adopted to automatically select the initiation points of the optimization routine. Shortly, the method discretizes first the parametric solution domain into sub-domains, and then locates the initiation points within the optimally selected sub-domains. After such a procedure, the initiation points come out as well-placed and un-clustered throughout the solution domain.

The number of initiation points is chosen by the user and it relates to (i) the space dimensions and (ii) the extension of the solution domain. While point (ii) may normally be handled by engineering judgment and expertise, the definition of point (i) keeps non trivial. The parameters to be taken into account within the matching procedure, and thus for defining the initiation point, are typically determined by SA (Saltelli et al. [39]). Sensitivity Analysis is widely used for model updating tasks and is considered as a necessary upstream step (Mottershead et al. [40]). However,

in its common application, it possesses the inherent inconsistency that SA is assessed on a fixed local point (initiation point), which may not coincide nor be near to the final (optimum) one. This clearly constitutes a drawback of the updating procedure. In fact, the initiation point may be "far away" from the optimum point and SA may point out to the appropriate underlying parameters located around the initiation point but not around the optimum one. This might lead to convergence problems or even to convergence failure. To avert this issue, the adoption of a LHS method is proposed here, first starting at the level of SA and then going to the level of global optimization. Also, the SA phase is analytically carried out, to avoid unwanted and costly approximations linked to numerical evaluations (e.g. through Finite Differences – FD) and to improve performance.

As a main reference to the salient points of the considered case study and of the self-implementation methodology, and to the original contributions of the present attempt, the following characteristic items may be outlined:

- The proposed updating procedure is herein developed and applied to a complete FEM model updating case study concerning a historic RC bridge with parabolic arches (1917), whose dynamic response has been first captured during an experimental vibrational campaign and then adopted as a benchmark reference for OMA modal identification and model updating purposes. A number of the identified modal properties of the structure is involved within the model updating procedure. Key structural parameters as Young's moduli and mass densities are located and consistently identified by the procedure, based on both natural frequency and mode shape estimations.

- The main original proposal of this paper consists in the comprehensive model updating investigation of the considered case study, which is handled by a self-implementation of an efficient LHS method to widely inspect the solution domain, in order to both perform a Sensitivity Analysis and to achieve a global optimization, in searching for potential multiple minima of the objective function, as revealed by a TR algorithm, and to derive a global optimum one. The benefits from the LHS implementation are illustrated throughout the paper. LHS indeed turns-out fundamental, for the present implementation purposes, since it does not require specific modifications of the optimization procedure itself and thus may also be implemented for a wide range of optimization problems.

- The whole updating procedure manages a fully automated interaction between mechanical FEM solver and numerical computing environment. This becomes very useful when necessary to consistently modify the FEM model to be updated (e.g. at the level of the boundary conditions or of the morphological characteristics). In this context, it is worthwhile to recall that in this work, in an effort to contain the computational burden of the updating procedure and to improve performance, the derivatives employed for the evaluation of the gradients of the objective function within the optimization problem are analytically determined.

The outline of the paper is as follows. Section 2 briefly introduces the theory of LHS and TR methods, as pertinent to the present implementation. Moreover, the FEM model updating procedure is presented and discussed. In particular, the objective function implemented into the optimization procedure is introduced, together with all SA-related aspects. Herein, the derivatives of the objective function adopted for the model updating are provided in their analytically determined form. Section 3 presents structural testing and modeling. Section 4 assesses the implemented model updating procedure, as applied to the present structural case study. Final comments on the effectiveness of the whole updating process within the present case study are pointed out in closing Section 5.

2 Optimization and updating implementation framework

2.1 Latin Hypercube Sampling and Trust-Region optimization

Latin Hypercube Sampling (LHS) originates from the field of statistics, McKay et al. [38]. It constitutes a sampling method originally designed to generate controlled random samples; in other

words, such a method is able to accurately recreate the input distribution through a sampling, in fewer iterations, when compared to classic random sampling (Monte Carlo method), characterized by the problem of clustering, whenever a small number of iterations is performed, Olsson et al. [41].

The LHS is based on the stratification of the probability distributions of each component of an M-dimensional vector of variables $\boldsymbol{\theta} = \{\theta^i,\, i = 1, \ldots, M\}$. Specifically, let the Cumulative Distribution Function (CDF) of each θ^i to be known and P the number of samples to be generated. Stratification divides the CDF curve into P equal intervals on the cumulative probability scale (0 to 1). Thus, the ranges of θ^i results to be partitioned into P intervals, of equal probability size $1/P$. Then, operating the Cartesian product of these intervals, domain $D \subseteq \mathbb{R}^M$ of $\boldsymbol{\theta}$ becomes divided into P^M cells, each of probability P^{-M}. A LH sample of size P is then obtained from a random selection of P cells among those partitioning D, according to the criteria of the so-called Latin Square rule (see Cavazzuti [42]). Hence, sampling is forced to represent values in each interval, and thus, to recreate the input probability distribution.

An intuitive representation of the LHS application in sampling procedures is provided in Fig. 1. In the figure, four points are (a) randomly generated and (b) automatically generated through the implementation of the LHS method in a 3D parametric space bounded between values $[0, 1]$ in each dimension. From this representation it is possible to observe that in case (b) the points appear as un-clustered and much well-spread, in filling the parametric domain, with respect to case (a). It is important to note that the LHS method for M variables and P points is independent from the specific application under consideration, and that, once the sampling of domain D for M variables and P points is formulated, a re-calculation of the sampling is not required.

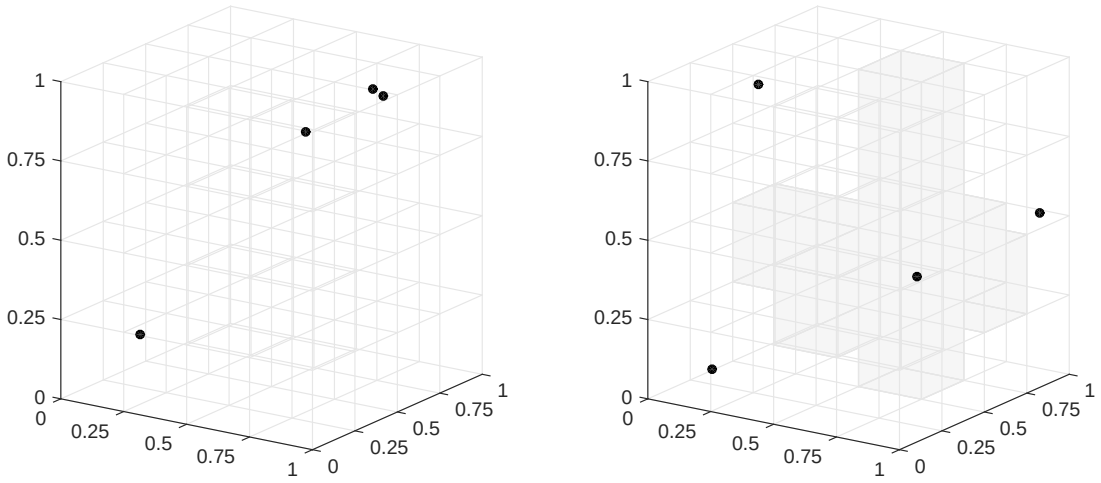

Figure 1: Latin Hypercube Sampling: (a) Non-LHS random distribution vs. (b) LHS-based automated distribution of four points in a $[0, 1]$-bounded 3D parametric space.

Trust-Region (TR) optimization may be used for deterministic model updating, in finding an optimum set of model parameters θ_i^* $(i = 1, \ldots, p)$ that minimizes a misfit between experimental data and model predictions, on a certain parametric space $D \subseteq \mathbb{R}^p$. Such a discrepancy is represented by a so-called *objective* or *cost function* $f(\boldsymbol{\theta})$. The model updating problem is thus equivalent to a nonlinear programming problem:

$$\boldsymbol{\theta}^* = \underset{\boldsymbol{\theta} \in D}{\arg\min} f(\boldsymbol{\theta}, \mathbf{d}) \tag{1}$$

where $\mathbf{d}$ is a given set of experimental data and $\boldsymbol{\theta}^*$ is the sought optimum solution. TR methods are used in mathematical optimization to search for a minimum of objective function $f(\boldsymbol{\theta})$, Nocedal and Wright [37], and define, around iterative current point $\boldsymbol{\theta}^k$, a confidence region, usually a hypersphere, assuming that there a local quadratic model may adequately represent the objective function. Then, the direction and extension (hypersphere radius Δ_k) of the step apt to minimize the local quadratic model are simultaneously determined and a new iterative point is set out.

In this study, according to a Matlab implementation with the adoption of the *lsqnonlin* function, the objective function is approximated in each trust region through a quadratic Taylor expansion model $m(\boldsymbol{\zeta}) = f(\boldsymbol{\theta}^k) + \nabla f(\boldsymbol{\theta}^k)^T \boldsymbol{\zeta} + \boldsymbol{\zeta}^T \mathbf{B}^k \boldsymbol{\zeta}/2$ where $\nabla f(\boldsymbol{\theta}^k)$ is the gradient vector of objective function $f(\boldsymbol{\theta})$ at current iterate $\boldsymbol{\theta}^k$ and $\mathbf{B}^k$ represents a suitable approximation of the Hessian matrix, so that $m(\boldsymbol{\theta}^k + \boldsymbol{\zeta}) \simeq f(\boldsymbol{\theta}^k + \boldsymbol{\zeta})$. At each iteration, the TR method then solves for the following (constrained) optimization sub-problem:

$$\boldsymbol{\zeta}^* = \underset{\|\boldsymbol{\zeta}\| \leq \Delta_k}{\arg\min}\ m(\boldsymbol{\zeta}) \tag{2}$$

The algorithm automatically sets the TR size, based on ratio $\rho_k = A_{red,k}/P_{red,k}$, where $A_{red,k}$ is the (actual) reduction in the objective function, while $P_{red,k}$ the (predicted) reduction in the approximated model. TR iterations are terminated once appropriate stopping criteria are met.

2.2 FEM model updating procedure

It is well known that, in model updating instances, if some of the requirements of objective function $f(\boldsymbol{\theta})$ are competing, multiple local minima of the optimization problem stated in Eq. (1) may exist, Mokhtar et al. [43]. As a consequence of such a lack of quasi-convexity of the objective function, the majority of the available local optimization algorithms, such as the above TR method, cannot guarantee that a global minimum may be found. In order to seek out the overall best solution, a global-scope search effort becomes thus imperative.

In this work, such an effort is attempted with regard to a "globalized" extension of a local search method. In particular, the TR method is herein considered, as follows. A number n of initiation points is first generated, as spread within the parametric (solution) domain. The TR algorithm is then used to perform as many optimization runs as the generated initiation points, providing, at the end of the (n) runs, a set of n solutions (local minima) $E = \{\boldsymbol{\theta}^{*,p},\ p = 1, \ldots, n\}$. The solution candidate to be the global one, $\bar{\boldsymbol{\theta}}^*$, is finally selected among the set of the obtained local minima ($\bar{\boldsymbol{\theta}}^* \in E$), through appropriate criteria.

The characteristics of set E are based on the mathematical properties of objective function $f(\boldsymbol{\theta})$ and on the initial population of initiation points. It is obvious that the higher the employed initiation points, the higher the probability to find a globally best solution, and that a convenient criterion to select the initiation points is mandatory to trust the global optimization procedure in leading to a successful solution.

As earlier stated in the Introduction, to comply with the above provisions, the above LHS sampling method is employed within the updating procedure, at two different levels: Sensitivity Analysis and global optimization.

First, the LHS method is implemented within a SA phase to set which parameters are to be contemplated within the updating procedure. This implies to define which parameters mostly influence the FEM modal response and, consequently, the dimensions of the parametric domain in which the optimization routine shall work. The advantages in using the LHS method relate to what follows. Sensitivity Analysis provides that derivatives of the FEM modal properties with respect to each characteristic parameter have to be evaluated: large or small values of such derivatives mean dependence or independence with respect to the selected parameter, respectively. However, modal derivatives are local quantities, i.e. they depend on the point where they are evaluated. If modal derivatives of a parameter are evaluated only at a certain point where, for instance, they result to be small, they will lead to the erroneous exclusion of that parameter from the optimization procedure. To avert this issue, modal derivatives with respect to each parameter must be evaluated at several points distributed within the whole parametric domain. Specifically, LHS is thus used to generate a set of N optimally spread initiation points (Section 2.1) within a parametric domain, dimensionally defined by the operator. From each sample obtained from LHS, a FEM eigenvalue problem is run and sensitivities are evaluated, computing a total number of N sensitivity matrices. Then, the average normalized relative sensitivity matrix is calculated. Based on the analysis on the components of such a matrix, the parameters that govern the modal response of the structure are finally established and selected as variables within the optimization routine. In doing so, the initiation point-localization dependence of SA is thus avoided.

Upon implementation at the level of SA, the LHS method is also used to define initiation points $\boldsymbol{\theta}^{0,p}$ from which the local optimization routine (TR) takes off, time after time, to finally search for potential multiple minima of the objective function. A careful selection of the point from which the optimization procedure takes off (initiation point) may increase the degree of confidence of the expected solution. Indeed, the closer this point to the solution, the higher the probability not to fall on a local minimum.

Sensitivity Analysis and definition of the initiation points, then constitute the *preprocessing* phase of the present optimization procedure. In a next step, the core of the optimization routine begins (*processing* phase). In particular, once the initiation point is defined, a FEM solver is involved to compute the structural response (here evaluated in terms of modal properties). Then, objective function $f(\boldsymbol{\theta}^k)$ and its gradient $\nabla f(\boldsymbol{\theta}^k)$ are calculated. Stopping criteria are checked, determining if current point $\boldsymbol{\theta}^k$ is the solution of the optimization path. If not, new point $\boldsymbol{\theta}^{k+1}$ is determined, through the TR method, and the optimization routine is repeated. The algorithm stops when specific stopping criteria are met.

2.2.1 Selection of global optimum

The selection of global minimum $\bar{\boldsymbol{\theta}}^* \in E$ may be performed according to different criteria. For instance, following a rigorous mathematical test, the global minimum should be the one providing the lowest value of the objective function. Another more engineering criterion may state that the choice should concern the point characterized by the least (minimum) value between the worst (maximum) errors on the frequencies among all local minima (*"minimax" criterion*). This specifically in view of the goal of refining as much as possible the eigenfrequency estimations, once predictions of the mode shapes are anyway being rather satisfactory. In this work, this last minimax criterion is applied as the rule of determining the best minimum point. This issue is further detailed in the applications later presented in Section 4.2.1.

The procedure so far described is illustrated in the synoptic flowchart reported in Fig. 2. The FEM model updating routine used in this work is implemented within MATLAB and function *lsqnonlin* is employed to manage the optimization process. ABAQUS may instead be involved as FEM solver; as an alternative, a FEM solver developed within MATLAB (Ferrari et al. [44–46]) may also be selected. This is actually a user choice, in the implemented updating procedure (see input block (parallelogram) in Fig. 2).

In following Section 2.3 the objective function considered in this study is presented. Afterward, Section 2.4 treats the Sensitivity Analysis based on which the parametrization of the solution domain and the calculation of gradient $\nabla f(\boldsymbol{\theta})$ for the TR implementation are determined.

2.3 Objective function for model updating

The objective function in model updating problems based on structural modal properties (see Eq. (1)) aims at achieving a close match between measured and computed modal parameters. Weighted least-squares formulations are commonly employed for the definition of the objective function (see e.g. Jang and Smyth [28], Simoen et al. [47]), as done in this study. Specifically, the objective function herein considered takes the following form:

$$f(\boldsymbol{\theta}) = \frac{1}{2}\left(\left(1 - \sum_{m=1}^{M} \alpha_m\right) \left\|\mathbf{r}^f(\boldsymbol{\theta})\right\|_2^2 + \sum_{m=1}^{M} \alpha_m \left\|\mathbf{r}^{s,m}(\boldsymbol{\theta})\right\|_2^2\right) \tag{3}$$

where the summation is performed over the M experimentally available modes, $\|\cdot\|_2$ is the Euclidean norm for vectors, $\boldsymbol{\theta}$ is the parameter vector to be optimized, $\mathbf{r}^f$ is the residual vector of the natural frequencies and $\mathbf{r}^{s,m}$ is the residual vector of the m^{th} mode shape. In detail, the latter two residuals are defined as follows:

$$r_m^f(\boldsymbol{\theta}) = \frac{\lambda_m(\boldsymbol{\theta})}{\tilde{\lambda}_m} - 1 \tag{4}$$

$$\mathbf{r}^{s,m}(\boldsymbol{\theta}) = \frac{\tilde{\phi}_l^m}{\phi_l^m}\,\boldsymbol{\phi}^m(\boldsymbol{\theta}) - \tilde{\boldsymbol{\phi}}^m \tag{5}$$

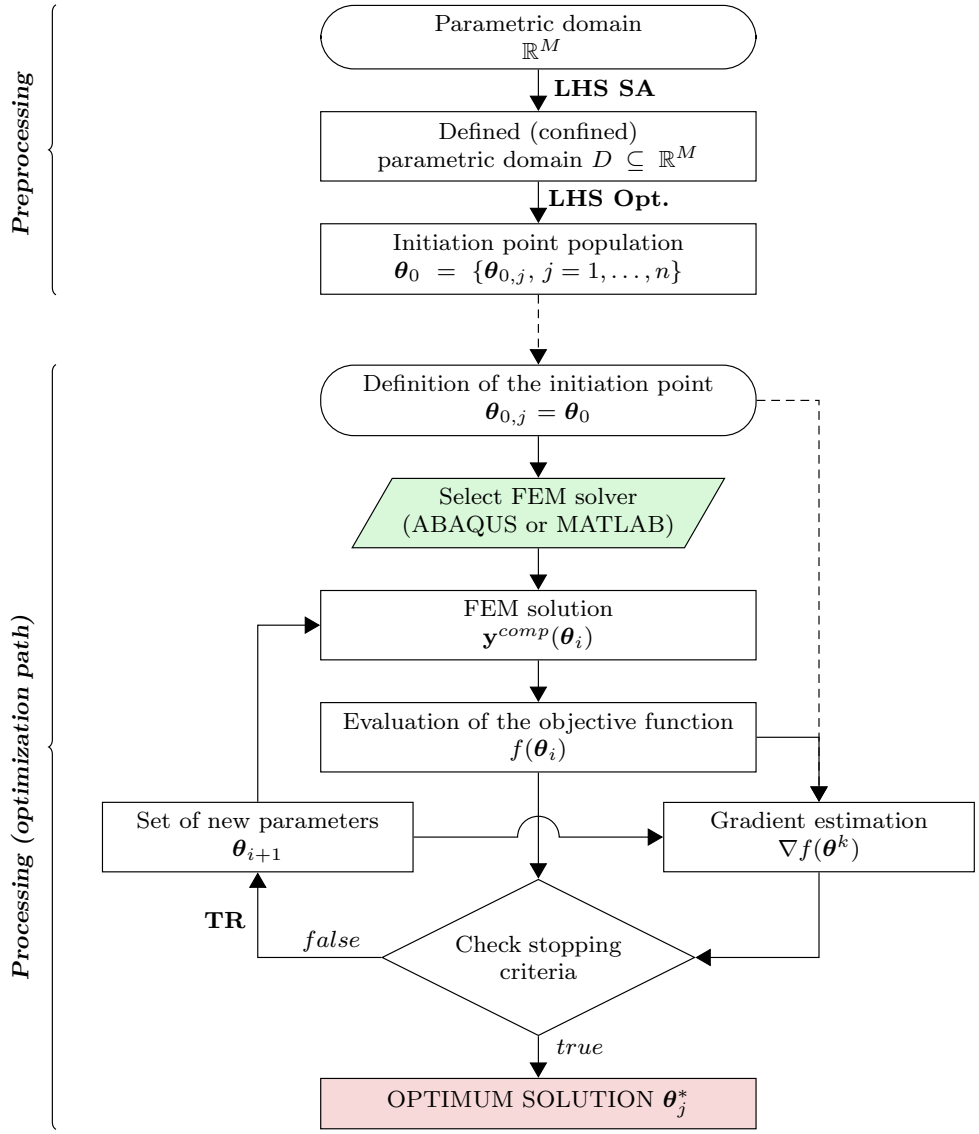

Figure 2: Flowchart of the LHS optimization process for FEM model updating

In Eq. (4), $\tilde{\lambda}_m$ and λ_m represent $(2\pi f_m)^2$ quantities (eigenvalues) related to identified and computed frequencies $\tilde{f}_m$ and f_m, respectively. In Eq. (5), $\tilde{\boldsymbol{\phi}}^m$ and $\boldsymbol{\phi}^m(\boldsymbol{\theta})$ are the identified and computed (eigenvectors) mode shape vectors, respectively. Since the computed mode shapes may display a different scale as compared to the identified ones, a scaling factor is applied on computed mode shape $\boldsymbol{\phi}^m(\boldsymbol{\theta})$; it is equal to the ratio between values $\tilde{\phi}_l^m$ and ϕ_l^m, which represent the maximum components of vector $\tilde{\boldsymbol{\phi}}^m$ and vector $\boldsymbol{\phi}^m$, respectively. It should be noted that such a scaling factor does not matter in the issue of avoiding a possible magnitude imbalance between the residuals of the natural frequencies and of the mode shapes that may appear in real calculations. This aspect has been taken into account in the implemented model updating procedure, in adopting the earlier mentioned *"minimax" criterion* (Section 2.2.1) on frequency residuals for determining the global minimum, thus effectively bypassing the possible problem of the above mentioned imbalance. Other approaches may be used as well to scale the mode shapes, such as the Modal Scale Factor (MSF), Shahverdi et al. [48]. This operator modifies the scale of the computed mode shapes, to minimize the difference with the maximum normalized identified mode shapes in a least-squares sense. However, as a drawback, it requires a very detailed description of the experimental mode shapes, Jang and Smyth [28].

In Eq. (3) α_m denote appropriate weighting coefficients ($\alpha_m \geq 0, \sum \alpha_m \leq 1$), shifting the importance of updating information on frequencies or on mode shapes (possibly based also on their availability or estimated accuracy), towards the purposes of the identification process. Notice that in Eq. (3) the relative differences are taken in the eigenvalue residual, in order to obtain a similar weight for each eigenvalue residual, due to the fact that, the higher the eigenvalue, the higher the absolute difference between analytical and experimental quantities. If, conversely, each natural frequency would be equally weighted in absolute terms, the algorithm would effectively weight more the higher eigenvalue. In the simulations presented later in the paper, values $\alpha_m = 1/(2M)$ have been assumed for all the M adopted modes, as a reasonable and consistent choice within the considered runs (see remarks later presented in Section 4.2.1, also concerning the considered criterion for selecting the global optimum solution devised in above Section 2.2.1, as applied to the present numerical investigation and pertinent results). As a matter of fact, it is worthwhile to remark that the presence of the mode shapes, within the updating process (i.e. within the objective function), is crucial to improve the prediction of the modal characteristics by the model updating, since they considerable enrich the amount and quality of the information coming from the targeted data (experimental modal features). On the other hand, once a good matching on the estimated mode shapes is achieved, keeping the chosen weight within the objective function, the criterion for the selection of the global minimum, which may be stated on the residual of the eigenfrequency estimation (Section 2.2.1), may selectively point out to a specific refinement of the frequency estimations, given the goodness of the predicted mode shapes. Moreover, when calculating the residual vectors, it is important to make sure that the comparison made between experimentally identified and numerically computed natural frequencies were made with frequencies corresponding to the same dynamic mode. This procedure is called *mode paring*. A classical Modal Assurance Criterion (MAC) value is used for the mode paring in this study.

In model updating schemes, it is often advantageous to select relative factors instead of the physical parameters themselves as parameters to be optimized, thus avoiding that largely varying orders of magnitude may induce numerical difficulties (inaccuracy) in the optimization procedure. To comply with this recommendation, for each considered physical parameter ϑ_i, the following corresponding relative non-dimensional factor is considered in the proposed procedure:

$$\psi_i = \frac{\vartheta_i}{\vartheta_i^0} \tag{6}$$

where ϑ_i^0 is the i^{th} physical parameter of a reference FEM base model. Thus, each ψ_i is expected to range at around 1, for all the model parameters.

As stated in Section 2.2, the TR method needs the calculation of the gradient of objective function $f(\boldsymbol{\theta})$. According to the expression of objective function $f(\boldsymbol{\theta})$ in Eq. (3), and the change of variables provided in Eq. (6), the gradient vector components result:

$$\nabla f_i(\boldsymbol{\psi}) = \frac{\partial f(\boldsymbol{\psi})}{\partial \psi_i} = \left(1 - \sum_{m=1}^{M} \alpha_m\right) r_j^f(\boldsymbol{\psi}) \frac{\partial r_j^f}{\partial \psi_i} + \sum_{m=1}^{M} \alpha_m \, r_j^{s,m}(\boldsymbol{\psi}) \frac{\partial r_j^{s,m}}{\partial \psi_i} \tag{7}$$

where implicit summation convention on repeated indices applies. By the chain rule, the derivatives of normalized residues $\mathbf{r}^f$ and $\mathbf{r}^{s,m}$ of Eqs. (4)–(5) are computed as follows:

$$\frac{\partial r_j^f}{\partial \psi_i} = \frac{\partial r_j^f}{\partial \lambda_k} \frac{\partial \lambda_k}{\partial \psi_i} = \frac{1}{\tilde{\lambda}_j} \frac{\partial \lambda_k}{\partial \psi_i} \tag{8}$$

$$\frac{\partial r_j^{s,m}}{\partial \psi_i} = \frac{\partial r_j^{s,m}}{\partial \boldsymbol{\phi}_k^m} \frac{\partial \boldsymbol{\phi}_k^m}{\partial \psi_i} = a_{jk}^m \frac{\partial \boldsymbol{\phi}_k^m}{\partial \psi_i} \tag{9}$$

In Eq. (9), matrix a_{jk}^m can be calculated as:

$$a_{jk}^m = \frac{\partial}{\partial \phi_k^m} \left(\frac{e_p^l \tilde{\phi}_p^m}{e_q^l \phi_q^m} \phi_j^m - \tilde{\phi}_j^m \right) = \frac{e_p^l \tilde{\phi}_p^m}{e_q^l \phi_q^m} \delta_{jk} - \phi_j^m \frac{e_p^l \tilde{\phi}_p^m \, e_q^l \delta_{qk}}{(e_q^l \phi_q^m)^2} = \frac{\tilde{\phi}_l^m}{\phi_l^m} \delta_{jk} - \frac{\tilde{\phi}_l^m}{(\phi_l^m)^2} \phi_j^m e_k^l \tag{10}$$

where $\mathbf{e}^l$ indicates the Cartesian unit vector with unitary l^{th} component and δ_{jk} is the Kronecker delta.

According to Friswell [49], the eigenvalue derivatives reported on the right hand side of Eq. (8) are evaluated by means of the following expression:

$$\frac{\partial \lambda_i}{\partial \psi_j} = \frac{1}{M_i} \boldsymbol{\phi}^{i\,T} \left(\frac{\partial \mathbf{K}}{\partial \psi_j} - \lambda_i \frac{\partial \mathbf{M}}{\partial \psi_j} \right) \boldsymbol{\phi}^i \tag{11}$$

where $\mathbf{K}$ and $\mathbf{M}$ are stiffness and mass matrices of the FEM model of the structure and λ_i and $M_i = \boldsymbol{\phi}_i^T \mathbf{M} \boldsymbol{\phi}_i$ are the eigenvalue and modal mass, of the i^{th} eigenmode, respectively.

On the other hand, a more involved procedure characterizes the calculation of the eigenvector derivatives reported on the right hand side of Eq. (9). In the algorithm herein proposed, the procedure presented by Nelson [50] is implemented.

As mentioned in the Introduction, the derivatives in Eqs. (8) and (9) are herein *"exactly"* determined, i.e. analytically, instead of by often-used Finite Differences (FD) numerical approximations. This way to operate is preferred for two main reasons. Firstly, the evaluation of such derivatives constitutes a mandatory task in gradient-based modal model updating and, therefore, approximations in their accounting may be avoided; secondly, the calculation through FDs is usually time-consuming. Considerable importance was given to this latter aspect, since it also concerns the SA phase, as described in the following section.

2.4 Sensitivity Analysis

The stability and well-posedness of gradient-based iterative methods for the solution of nonlinear optimization problems are crucially related to the conditioning of approximated Hessian matrix $\mathbf{B}^k$ (see Section 2.1), which depends, in turn, on the gradient of the objective function. Ill-conditioning of the Hessian matrix may be extremely common in model updating, resulting in a solution which is very unstable with respect to small changes in the model predictions and in the data vector.

An effective expedient to prevent this problem lies in avoiding near-zero components in gradient vector $\nabla f(\boldsymbol{\theta})$ and over-parametrization along the structure, which produces nearly linearly dependent columns in the Jacobian matrix for the neighboring elements. This translates into the selection, for the model updating, of those physically relevant parameters of the FEM model that sufficiently affect the observed data, i.e., the selection of a reasonable initiation point for the optimization process, Brownjohn et al. [51].

In order to asses which parameters markedly affect the structural response, thus avoiding consequent ill-conditioning troubles, SA is carried out. The selection of the parameters to be updated is a decisive moment within the model updating procedure, and the analysis of sensitivity matrix $\mathbf{S}$ constitutes an efficient tool, allowing for the selection of the parameters that most influence the structural response.

In modal vibration-based model updating, the required sensitivities relate the predicted eigenvalues and eigenvectors to the unknown structural parameters. In this study, SA is based on the predicted eigenvalues. Thus, it turns out that the sensitivity matrix corresponds to Eq. (11), namely:

$$S_{ij}(\boldsymbol{\psi}) = \frac{\partial \lambda_i(\boldsymbol{\psi})}{\partial \psi_j} \tag{12}$$

where it is reiterated that λ_i represents a specific eigenvalue and ψ_j is defined by Eq. (6), with $i = 1, \ldots, M$, for M considered eigenvalues and $j = 1, \ldots, N$ for N structural parameters. Since sensitivities related to different quantities have to be compared, the following normalized relative sensitivity matrix $\mathbf{S}_n$ is specifically employed:

$$S_{n\,ij}(\boldsymbol{\psi}) = \frac{1}{\lambda_i} \frac{\partial \lambda_i}{\partial \psi_j} = \frac{1}{\lambda_i\, M_i} \boldsymbol{\phi}^{i\,T} \left(\frac{\partial \mathbf{K}}{\partial \psi_j} - \lambda_i \frac{\partial \mathbf{M}}{\partial \psi_j} \right) \boldsymbol{\phi}^i \tag{13}$$

As described above, in the present updating procedure the sensitivities in Eq. (13) are determined for each of the optimally located points automatically generated by the LHS method within the parametric domain, and their average is evaluated. Thus, the average $\mathbf{S}_n$ matrix is calculated and the parameters that govern the modal response of the structure are then established and selected as underlying variables within the optimization routine.

3 Testing and modeling of Brivio bridge (1917)

3.1 Brief description of the bridge

The historic Brivio Bridge (Santarella and Miozzi [52], Froio and Zanchi [53]) is a three-span RC arch bridge located between Brivio (province of Lecco, LC) and Cisano Bergamasco (province of Bergamo, BG), in the Lombardia region, northern Italy. Built in 1917, the bridge crosses the Adda river at an approximate height of 8 m from water (Fig. 3). The bridge consists of three spans, with characteristic parabolic arches and is fully symmetric with respect to its mid-longitudinal plane. The central span is 44 m long, while the lateral spans linked to the river banks are 43.4 m long, totaling to a length of 130.8 m. The road deck is 9.2 m wide and hosts two roadway lanes and two cantilever sidewalks, 0.8 m wide. The deck of each span of the bridge includes two main longitudinal girders (0.45 m $\times$ 1.00 m) placed at a respective transverse distance of 8.60 m, and two further secondary beams (0.20 m $\times$ 0.55 m) placed at a distance of 2 m, symmetrically located with respect to the vertical longitudinal plane of the bridge. Between these girders, transverse beam connections (0.30 m $\times$ 0.75 m) are placed at approximately every 2.30 m. The resulting structural grid supports a RC slab of 0.15 m of depth.

The characteristic arches of the bridge feature a 42.80 m span and a rise of 8.00 m. Each arch presents a rectangular cross section, characterized by a constant width, equal to 0.60 m, and a height varying from 1.25 m (in the middle) to 1.37 m (at the ends). The profile of the arch is symmetric with respect to the vertical axis at half span. The arches are linked to each other on their upper central part by eight transverse beams and to the deck by means of sixteen RC hangers per side, per span, of rectangular cross section (0.32 m $\times$ 0.60 m).

Two concrete piers constitute the intermediate supports of the deck into the river bed. The piers are tapered, with maximum dimensions at the base of 12.8 m along the transverse direction of the bridge and of 3.8 m along its longitudinal direction. Each pier rests on forty-eight RC piles driven into the river bed, ranging from 13 m to 16 m in depth; each pile displays a square cross section of 0.35 m. Above both the intermediate piers and the abutments, a RC slab of 1 m height is placed.

Figure 3: Present downstream view of three-span Brivio bridge (1917) on river Adda; Brivio (LC) right bank (left), Cisano Bergamasco (BG) left bank (right).

3.2 Testing and system identification of the bridge

Experimental campaigns were carried out on the bridge on 11–13 June 2014. During the tests, several instrumentations were used (see Ferrari et al. [14,15]), including standard wired accelerometers, for collecting the accelerations of the structure under current traffic load. Such accelerometers were installed on the bridge as an integrated system composed of: (a) a 24-channel data acquisition system, comprising of 6 NI 9234 4-channel dynamic signal acquisition modules (24-bit resolution, 102 dB dynamic range and anti-aliasing filters), interfaced to a remote PC and to its storage unit; (b) uniaxial WR 731A piezoelectric accelerometers on the roadway deck; each WR 731A

sensor, capable of measuring accelerations up to 0.5 g with a sensitivity of 10 V/g, was connected with a short cable to a WR P31 power unit/amplifier. Data were collected at a sampling rate of 200 Hz. Accelerometers were placed on both sides of the deck to capture both bending and torsion responses, according to the two setups shown in Fig. 4. Two time series of 3600 s were recorded per each setup, to ensure a good data quality. In this paper, measurements derived from the span of the bridge placed on the Brivio side (hereafter referred to as first span, i.e. left span in Figs. 3 and 4) are employed for the ensuing discussion.

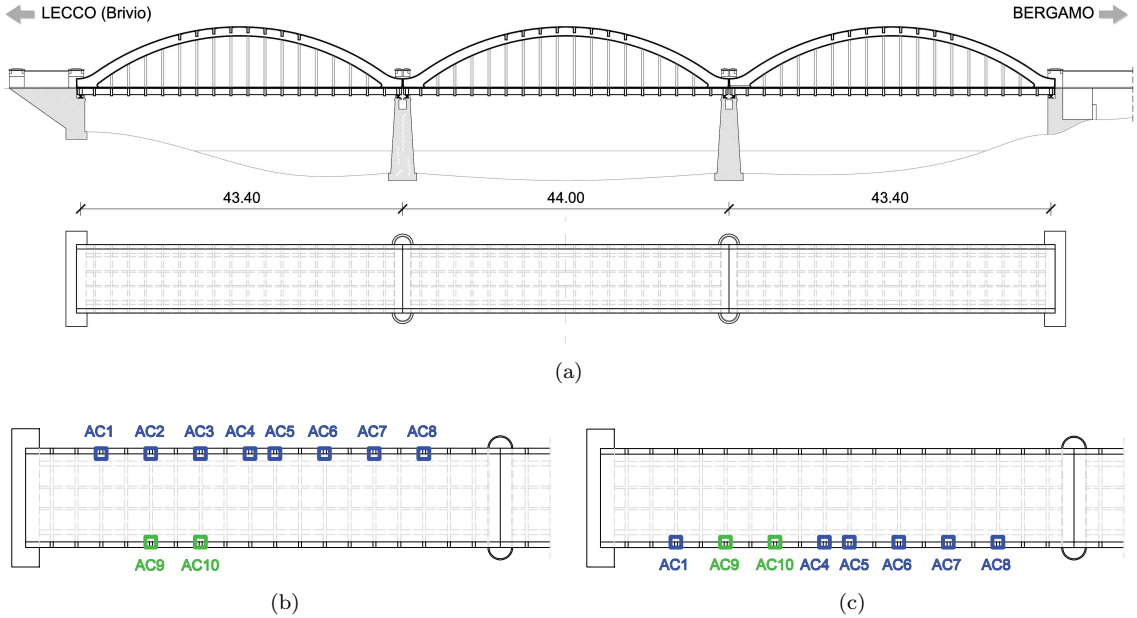

Figure 4: Schematic downstream front and top views of Brivio bridge (a) and accelerometer location for the vibration-based recording with two setups (b),(c). Dimensions in meters.

For system identification in the frequency domain, a standard Frequency Domain Decomposition (FDD) method (Brincker et al. [54]) has been used. The obtained results are represented in Fig. 5 in terms of the natural frequencies, which can be discerned from the local maxima of the first Singular Value (SV) line. The corresponding mode shapes follow in Fig. 6. For cross-checking the results of peak picking, a standard data-driven Stochastic Subspace Identification (SSI-data) method (Peeters and De Roeck [55]) has also been adopted, allowing as well for the damping ratio estimations (see also Pioldi and Rizzi [56,57], for a recent comparison of the the two OMA methods, in enhanced forms). Table 1 summarizes the natural frequencies consistently identified from the FDD and SSI methods, together with the damping ratios identified by the SSI method.

Table 1: Experimentally identified modal frequencies (FDD and SSI methods) and damping ratios (SSI method), and mutual MAC indexes.

Mode	**1**	**2**	**3**	**4**	**5**	**6**	**7**	**8**	**9**
$f^{\mathbf{FDD}}$ [Hz]	3.564	3.857	6.018	7.178	7.690	9.009	11.38	13.09	17.02
$f^{\mathbf{SSI}}$ [Hz]	3.449	3.887	5.968	7.146	7.592	8.928	11.39	13.04	16.99
$\Delta f^{\mathbf{exp}}$ [%]	−3.23	0.78	−0.83	−0.45	−1.27	−0.90	0.11	−0.35	−0.16
$\zeta^{\mathbf{SSI}}$ [%]	4.60	4.09	3.17	1.51	2.82	1.67	1.28	2.01	1.44
MAC	0.997	0.991	0.998	0.989	0.991	0.990	0.938	0.987	0.935

In Table 1, it can be appreciated that the modal frequencies identified by both OMA methods match each other quite well and that there appear values above 0.93 for all the mutual MAC indexes. Indeed, the absolute value of percentage discrepancy Δf^{exp} that exists between the frequencies determined through the FDD method and the SSI method, with respect to the FDD estimates ($\Delta f^{\text{exp}} = (f^{\text{SSI}} - f^{FDD})/f^{FDD}$) does not exceed 3.23% (see Table 1).

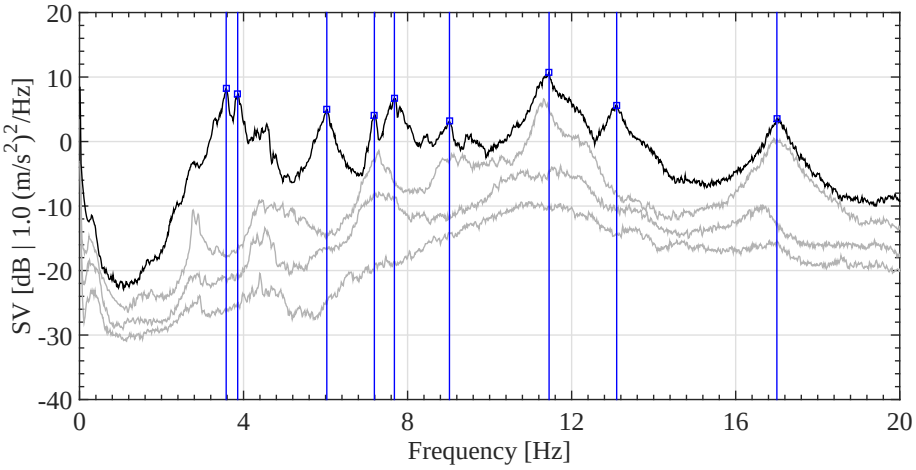

Figure 5: SV curves resulting from classical FDD.

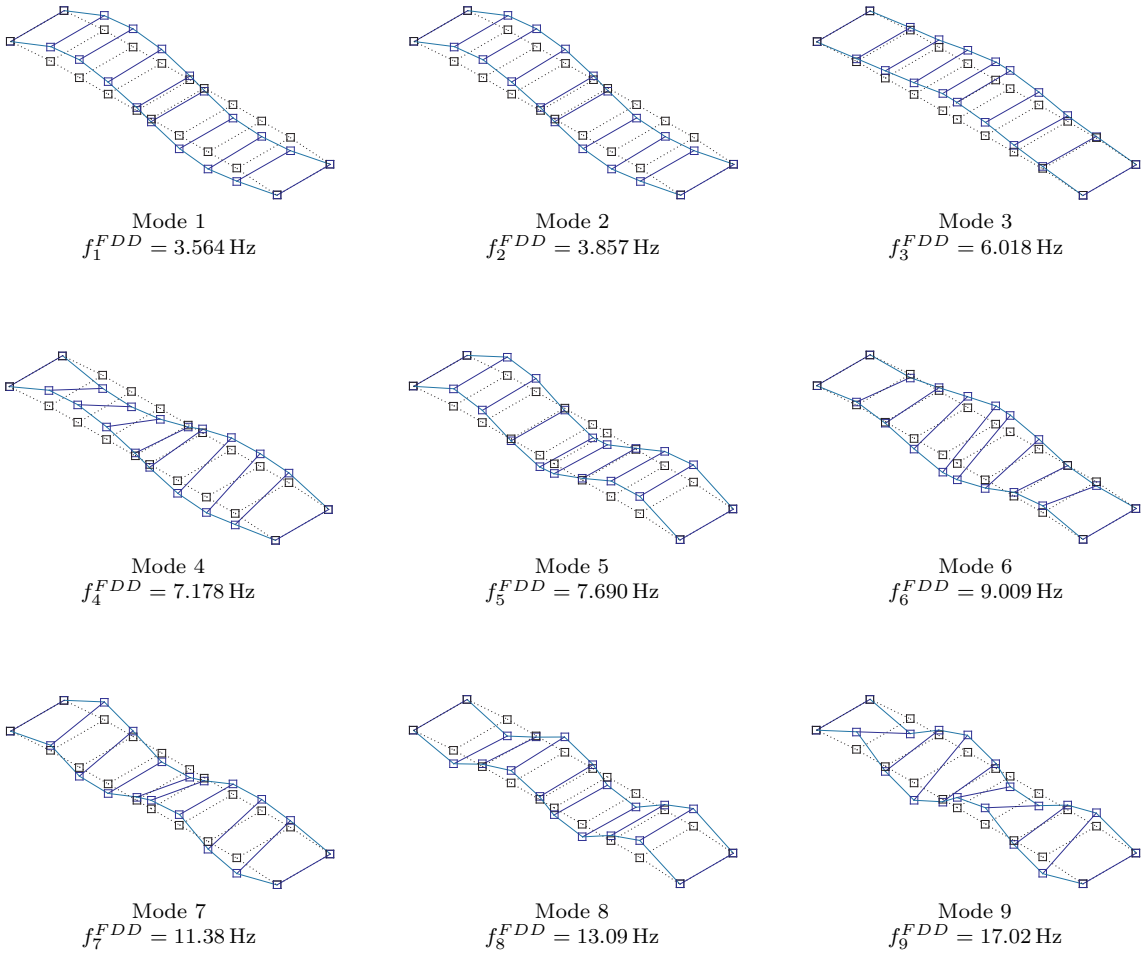

Figure 6: Mode shapes corresponding to the identified modal frequencies listed in Table 1 (FDD).

Figs. 6–7 show the mode shapes of the first span of the bridge as identified by the FDD method, represented also through polar plots in Fig. 7. From Fig. 6, it can be observed that almost all the mode shapes exhibit regular and smooth shapes, dominated by bending and/or torsion, with the

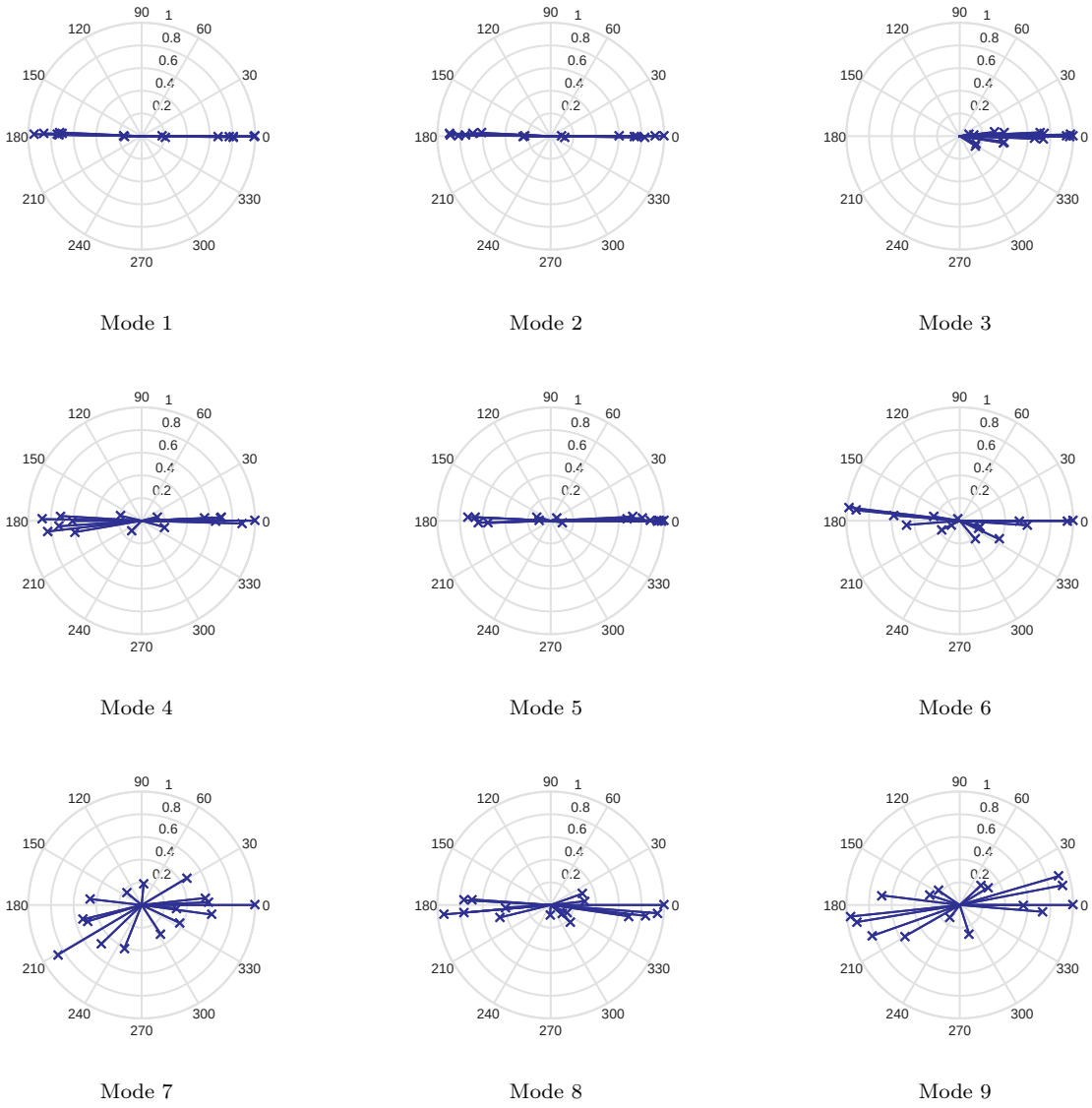

Figure 7: Polar plots for the mode shapes corresponding to the identified natural frequencies listed in Table 1 (FDD). Main complex components appear only for Modes 7 and 9.

exception of the 7th mode, which is characterized by coupled bending and torsion.

Moreover, although Modes 1 and 2 are associated to different frequencies, they exhibit a practically identical experimentally obtained mode shape. This occurrence, also referred to as "frequency splitting phenomenon" (Zonta and Modena [58]), was also pointed out in preliminary analyses conducted on the Brivio bridge (see Ferrari et al. [15]), where this was associated to the possible presence of damage (see Ubertini et al. [59]), such as linked to cracking of some vertical hangers. As a further consideration, the observed phenomenon may also be linked to the presence of added mass due to the transiting vehicles (consisting also on several trucks, during the prolonged acceleration recordings, sometimes crossing at slow speed or even standing in line, with the traffic on the bridge), leading to display a splitting of the modes as in Tuned Mass Damper (TMD) passive vibration mitigation/control device tuning and identification (as for instance reported by Wang and Lin [60], and in general terms about TMD tuning in Salvi and Rizzi [61–63], with references quoted therein). Another physical interpretation could be related to the presence of a slight coupling of the modes of the three different spans. This could have been revealed by additional vibrational acquisitions on the other two spans, or by means of numerical simulations

comprising the whole bridge structure. The latter choice would of course complicate the matching between the experimental evidence and the model response, in this way merely translating the problem to potential numerical convergence issues. However, giving right to a numerical model interpretation, the subsequent modal analysis performed through the FEM model of the first span of the bridge shows the presence of an additional mode close to the first one and quite similar to that in terms of deck bending but involving also a torsional component of the whole structure (see following Figs. 9 and 16). This has led to conduct, in the present investigation, two different model updating procedures. The points considered on this specific aspect are outlined in Section 4.1.1. All these interpretative conjectures may be further assessed by additional investigations, possibly requiring further experimental campaigns on the bridge, if they would later become possible.

The modal properties (frequencies and mode shapes) estimated from the FDD algorithm are here assumed as the identification target for the model updating process that follows. This is because they are felt as readily visible and accessible (Fig. 5), and as rather reliable, in both frequencies and mode shapes, also after sample consistent validations with separate refined FDD evaluations (Pioldi et al. [10–12]), providing a higher comfortable level of personal confidence for the following purposes of model updating. Despite, the alternative predictions from SSI OMA identification could also be assumed for the following model updating analysis.

3.3 FEM model of the bridge

Brivio bridge (first span) has been modeled through a linear elastic FEM model, first implemented within ABAQUS (Froio and Zanchi [53], Ferrari et al. [17]), and later transported into a separate FEM MATLAB implementation. It consists of a 3D frame structure with beam elements, mutually connected at the nodes. It is obtained as an assembly of four main sub-structures, namely deck, arches, hangers and upper transverse beams. The FEM model of the bridge is shown in Fig. 8; in such a sketch, the x-, y- and z- axes represent the longitudinal axis, the vertical axis and the horizontal transverse axis of the bridge, respectively.

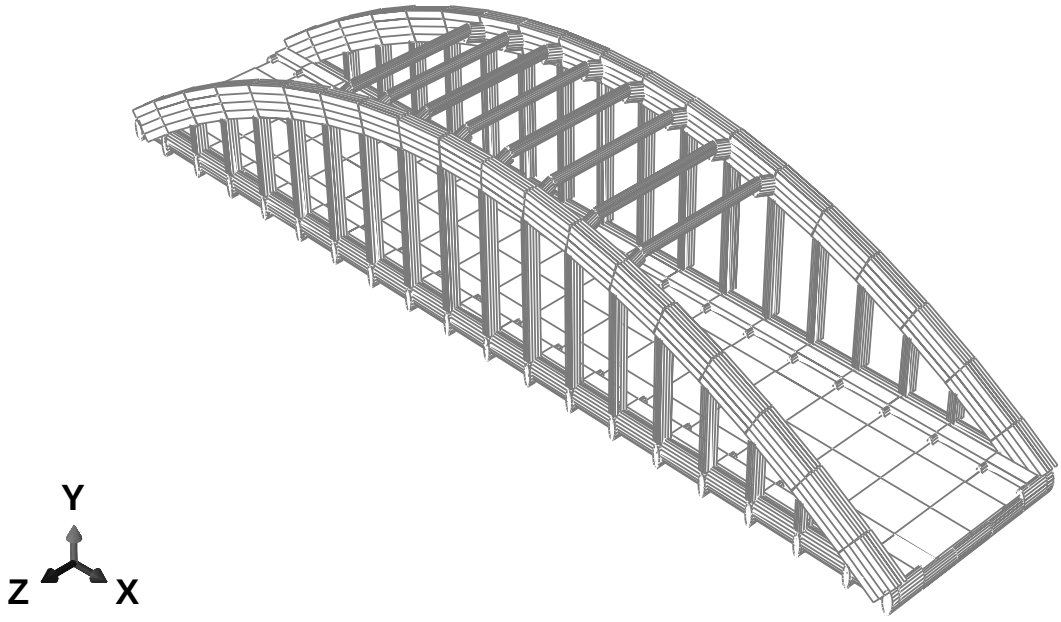

Figure 8: FEM model of Brivio bridge (single span, with rendering of the beam profiles).

The geometry of the FEM model has been carefully deciphered based on available design drawings of the bridge. Since it has been preferred not to consider geometry characteristics within the updating procedure, a very careful attention has been paid on this. The cross-sectional area and the moments of inertia have been calculated based on the design drawings. In case of lack of information about dimensions, reasonable guesses have been made, also based on a local inspection

and photographing. The deck is modeled as a framework of 254 beams, the arches are made of 70 elements, whereas 24 elements constitute the upper beams. The deck-hanger and the hanger-arch joints are modeled by using rigid links. A non-structural component referring to the asphalt layer is also included in the model, as an added mass, as uniformly distributed along the deck of the bridge.

Concerning the boundary conditions, the model is considered as simply supported at one extremity of the deck and four different types of linear springs are considered to be located as follows: two z-axis rotational springs are placed at both extremities; two translational springs, one horizontal (x-axis) and one vertical (y-axis), are located at the second extremity. These rotational and translational springs are inserted for modeling the possible interaction of span 1 with the neighboring span and for compliance with the presence of the concrete pier at the extremity of the beam, respectively.

The final 3D FEM model of the bridge counts for 380 beam elements, 280 structural nodes and 1680 degrees of freedom (nodal displacements and rotations, after assembly) and is implemented as fully symmetric with respect to the vertical longitudinal plane of the structure.

4 FEM model updating of Brivio bridge

4.1 Parametrization of the updating problem

To parametrize the updating problem here refers to define the characteristic parameters to be considered as "eligible" variables for the problem itself, namely the parameters that can be selected as variables of the optimization procedure that such problem implies (see Section 2). This selection precedes SA, under which, however, the effective parameters that will be updated during the optimization process are selected among all the variables that characterize (parametrize) the updating problem. SA for the Brivio bridge is treated in following Section 4.1.1.

For the present case study, a total of 14 variables is outlined at this stage to parametrize the updating procedure. In particular, 10 variables refer to 5 Young's moduli and 5 mass densities of the five substructures in which the FEM model of the bridge is subdivided (Section 3.3), based on the morphological and topological characteristics of the structure (i.e., deck, main longitudinal girders, parabolic arches, hangers, upper transverse beams); 4 additional variables refer to the stiffness coefficients of the springs considered for modeling the bridge's boundary conditions (Section 3.3).

In a first stage of the study, the asphalt layer originally included in the model was considered for the parametrization of the updating problem, since it was supposed to be important for a successful optimization procedure. Preliminary runs of the code were then processed considering an added mass for simulating the asphalt layer and thus, considering the density of such a mass as an additional parameter to be updated. Simulations returned specific values of the problem's variables, based on which the modal characteristics of the (updated) FEM model were then determined. At a later stage, additional simulations were performed without considering added masses for modeling the asphalt layer. In this case, the optimization process updated the density of the deck, by making the final mass of the latter equal to the mass obtained in the prior simulations, as the sum of the mass of the deck and the mass of the asphalt layer. At this second stage of analysis, results equal to those obtained in the first simulations were obtained in terms of the modal characteristics of the bridge. On that basis, and in order to avoid an over-parametrization of the updating problem, the uniformly distributed added mass on the deck of the bridge was thus removed from the FEM model, leaving the optimization process in charge to modify (update) the density of the deck, in order to cover the increment of mass provided by the asphalt layer. No variables were thus added on that for the parametrization of the updating problem.

The 14 variables above selected to parametrize the updating problem are listed in Table 2, along with their baseline values (reference values) assigned to such variables in order to check the similarity between experimental and (initial) FEM model behavior. The baseline values have been set by trying to minimize, through a *"manual tuning"* process, the discrepancies between the first two, numerical and experimental, modal frequencies. Moreover, in view of implementing the updating procedure, lower and upper bound values have been set to define the solution domain of the optimization process. The bounds have been outlined based on engineering judgment, allowing for the natural frequencies of the FEM model of the bridge to reasonably vary, but not to

Table 2: Input parameters of the FEM base model.

Parameter			Bounds			
No.	**Description**	**Symbol**	**Lower**	**Upper**	**Ref. value**	**Units**
P1	Deck elastic modulus	E_d	24.4	45.4	34.9	GPa
P2	Main longitudinal girders elastic modulus	E_{lg}	24.4	45.4	34.9	GPa
P3	Parabolic arches elastic modulus	E_a	25.0	46.4	35.7	GPa
P4	Hangers elastic modulus	E_h	25.0	46.4	35.7	GPa
P5	Upper transverse beams elastic modulus	E_{ub}	25.0	46.4	35.7	GPa
P6	Deck mass density	ρ_d	1.71	3.17	2.44	t/m^3
P7	Main longitudinal girders mass density	ρ_{lg}	1.71	3.17	2.44	t/m^3
P8	Parabolic arches mass density	ρ_a	1.71	3.17	2.44	t/m^3
P9	Hangers mass density	ρ_h	1.71	3.17	2.44	t/m^3
P10	Upper transverse beams mass density	ρ_{ub}	1.71	3.17	2.44	t/m^3
P11	I-support translational (x-axis) spring stiffness	k_1	10^{-7}	10^{-3}	10^{-5}	kN/m
P12	I-support translational (y-axis) spring stiffness	k_2	10^{8}	10^{12}	10^{10}	kN/m
P13	I-support rotational spring stiffness	k_3	10^{-7}	10^{-3}	10^{-5}	kN m
P14	II-support rotational spring stiffness	k_4	10^{-7}	10^{-3}	10^{-5}	kN m

diverge much from the identified ones. Specifically, a variation range of the values of the variables between -30% and $+30\%$ has been considered. Given the uncertainty in evaluating the boundary conditions, wide ranges of variation of spring stiffnesses are allowed, by four orders of magnitude, and simply referring to values in terms of orders of magnitude, with a reference value right in the middle of the considered orders of magnitude (see also hints from the literature, e.g. Aktan et al. [64], and experience gained in previous trials by Froio and Zanchi [53] and Ferrari et al. [17]).

This quite large variation range of the parameters has been considered due to the considerable age of the structure of interest and to the lack of further information linked to the mechanical parameters of the bridge that may arise from direct detailed inspections on the bridge or from other approaches apt to handle these issues, e.g. Non-Destructive Testing. Also, the wide range is accounted for to inspect the authentic potentialities and effectiveness of the optimization process. Of course, such a range could then be a-posteriori reduced, around the target values, or varied, by further refinements of the proposed updating procedure.

Table 3: Comparison between experimental (identified) and numerical (FEM base model) modal properties.

Mode	**Description**		**Identified freq. (FDD) [Hz]**	**FEM base model freq. [Hz]**	**Δf^{bm} [%]**	**Mutual MAC**
V1	1^{st}	bending	3.564	3.785	6.20	0.9986
T1	*1st*	*torsion*	*3.857*	*4.040*	*4.74*	*0.0424*
V2	2^{nd}	bending	6.018	5.914	−1.73	0.9921
T2	2^{nd}	torsion	7.178	6.523	−9.13	0.9913
V3	3^{rd}	bending	7.690	7.856	2.16	0.9951
T3	3^{rd}	torsion	9.009	8.904	−1.17	0.9340
T4	4^{th}	torsion	11.38	10.66	−6.31	0.6859
V4	4^{th}	bending	13.09	12.33	−5.84	0.9721
T5	5^{th}	torsion	17.02	15.74	−7.51	0.9627

Table 3 and Fig. 9 show the results of modal analysis performed through the FEM model of the bridge characterized by the reference values listed in Table 2 (hereinafter referred to as *FEM base model*). Specifically, in Table 3 the natural frequencies from the FEM base model and the correlation between the dynamic characteristics of the base model and the experimental results are reported, showing the relative frequency discrepancy ($\Delta f^{\mathrm{bm}} = (f^{\mathrm{bm}} - f^{FDD})/f^{FDD}$) and the mutual MAC value.

From the obtained results it is possible to note that Mode 1 and Mode 2 present modal frequency values close to each other. However, contrary to what was obtained from the experimental results, such modes differ in mode shapes; in fact, the first mode shape appears dominated by bending, while the second one by torsion (see Fig. 9), being almost orthogonal. This is also reported by the only abnormal (almost vanishing) MAC value obtained for the second (first torsion)

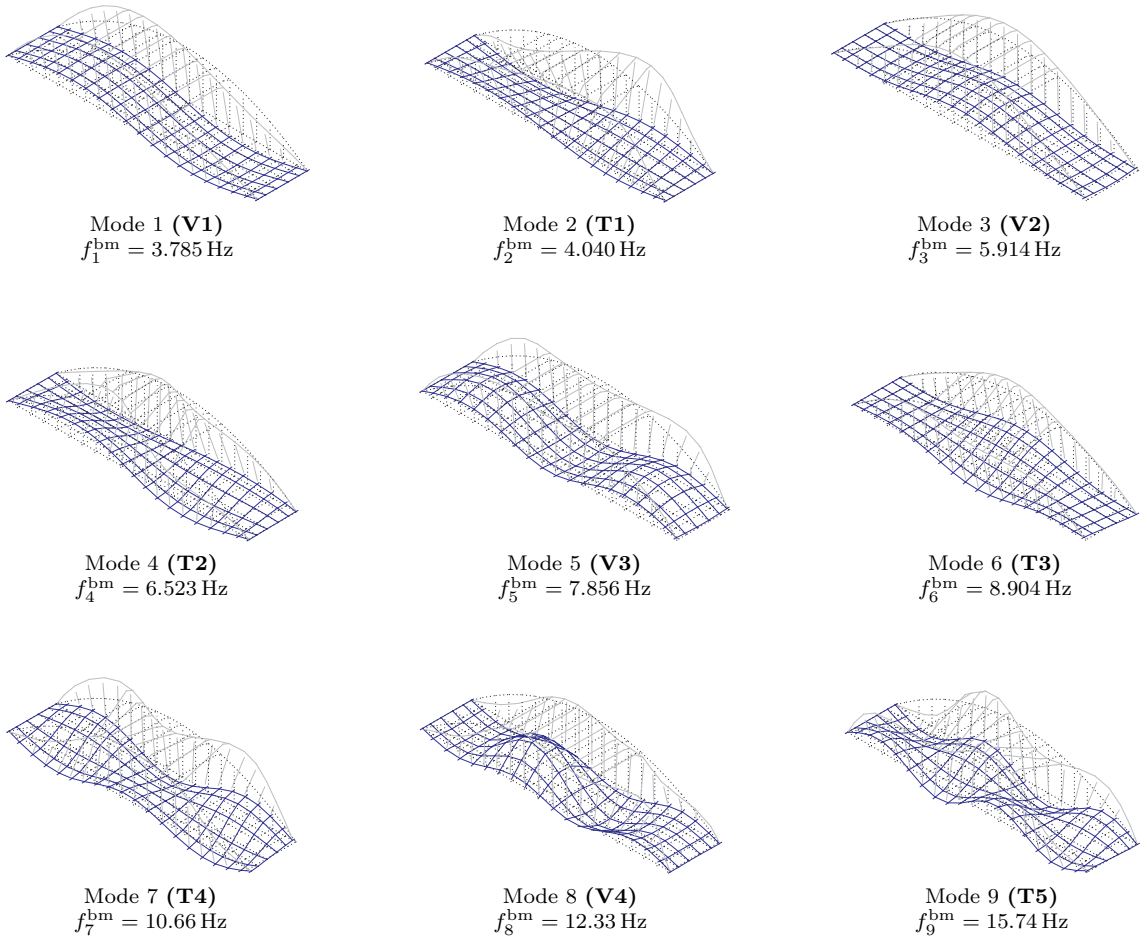

Figure 9: Natural frequencies f_i^{bm} and mode shapes of the FEM base model (bm) of the bridge (not updated) corresponding to the nine identified modes.

mode (T1) (Table 3). Moreover, for the nine modes, the relative errors in the natural frequencies reasonably range between 1.17% and 9.13%, thus they are all below a 10% discrepancy. With the exception of mode T1, the first five numerical modes display MAC values higher than 0.99; further, modes T3, V4 and T5 display MAC values higher than 0.93. In addition to the second mode, there appears only one mode with a MAC lower than 0.70, namely 7^{th} mode T4, endowed with complex components if Fig. 7. The MAC paring matrix between experimental and computed mode shapes of the FEM base model of the bridge before updating is depicted in Fig. 10, already showing a rather good correlation. Overall, the modal features generally show a fairly good correlation between experimental data and numerical results from the FEM base model; the accuracy paid to the initial definition of the FEM base model definitely played a crucial role in reaching such a result. This constitutes the basis of the subsequent model updating process.

In the present model updating study, analyses were then conducted for two main cases:

- (A) excluding Mode 2 from the procedure (use of 8 modes);
- (B) including both Mode 1 and Mode 2 into the optimization routine as a target for the updating procedure (use of 9 modes).

Whereas results for Case (A) turned out rather satisfactory, results for Case (B) were not. This has lead to support the conjecture that the second mode identified from the experimental tests performed on the bridge may actually correspond to a splitting of the first mode or to an uncorrect identification of its torsion component (see extensive discussion at the end of Section 3.2).

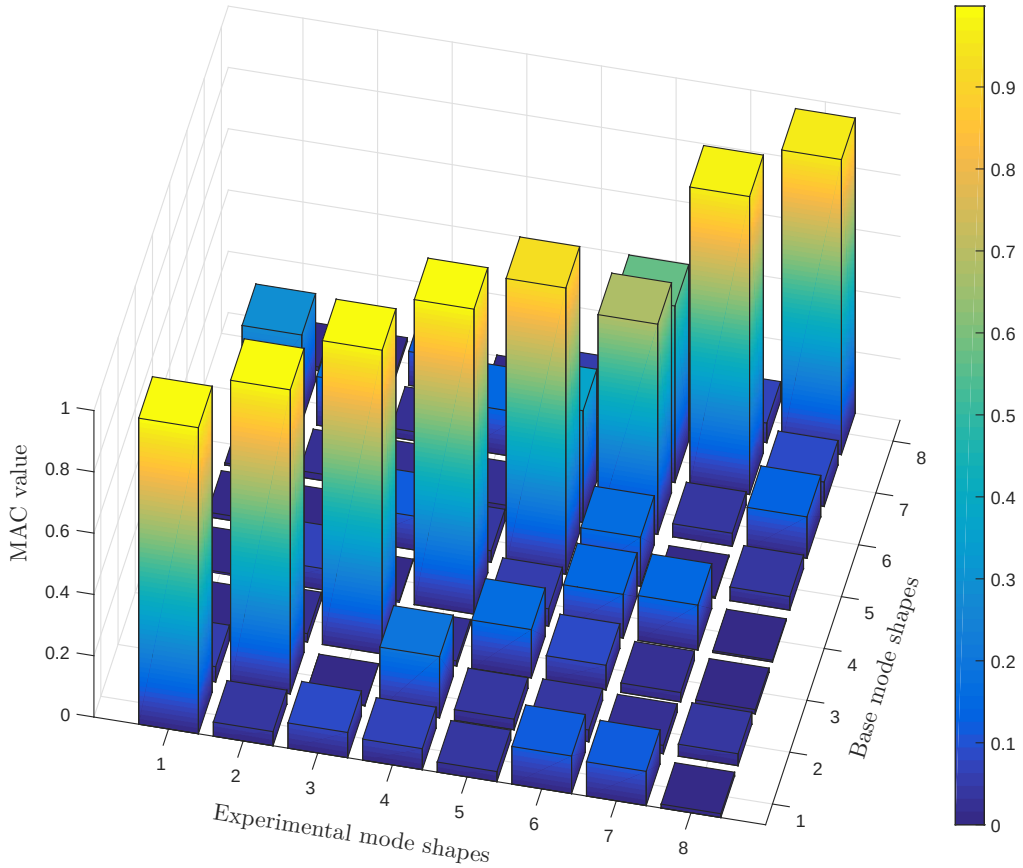

Figure 10: MAC paring matrix between considered eight experimental and computed mode shapes before model updating (FEM base model).

Nonetheless, the presence of an "additional" mode reported by the FEM base model of the bridge corresponding to the second experimentally identified frequency leaves the door open for further studies that may be conducted on this specific issue, possibly based on further experimental outcomes, if they may become available.

In light of the considerations above, in the paper only consistent model updating results for Case (A), based on eight modal properties, and revealed in appearance on nine FEM modes, are consistently reported, as detailed in subsequent Section 4.2 (see later final updated Table 8 vs. Table 3, and Fig. 16 vs. Fig. 9).

4.1.1 Sensitivity Analysis results

Following the preliminary modal analysis, a Sensitivity Analysis on the variation of the natural frequencies has been performed with respect to the 14 parameters that characterize the updating problem. Sensitivities have been calculated as explained in Section 2.4. First, the LHS method has been applied to select 20 combinations of the parameters in the ranges within the bounds listed in Table 2; then, the average normalized relative sensitivity matrix (Eqs. (10) and (11)) has been calculated over the sensitivities for the 20 combinations. The recorded dispersion of the local sensitivities with respect to the average ones is similar to that discussed below (end of the subsection), for the differences evaluated between the local sensitivities on the initiation points and the average values. A graphical representation of the average sensitivity matrix is provided in Fig. 11.

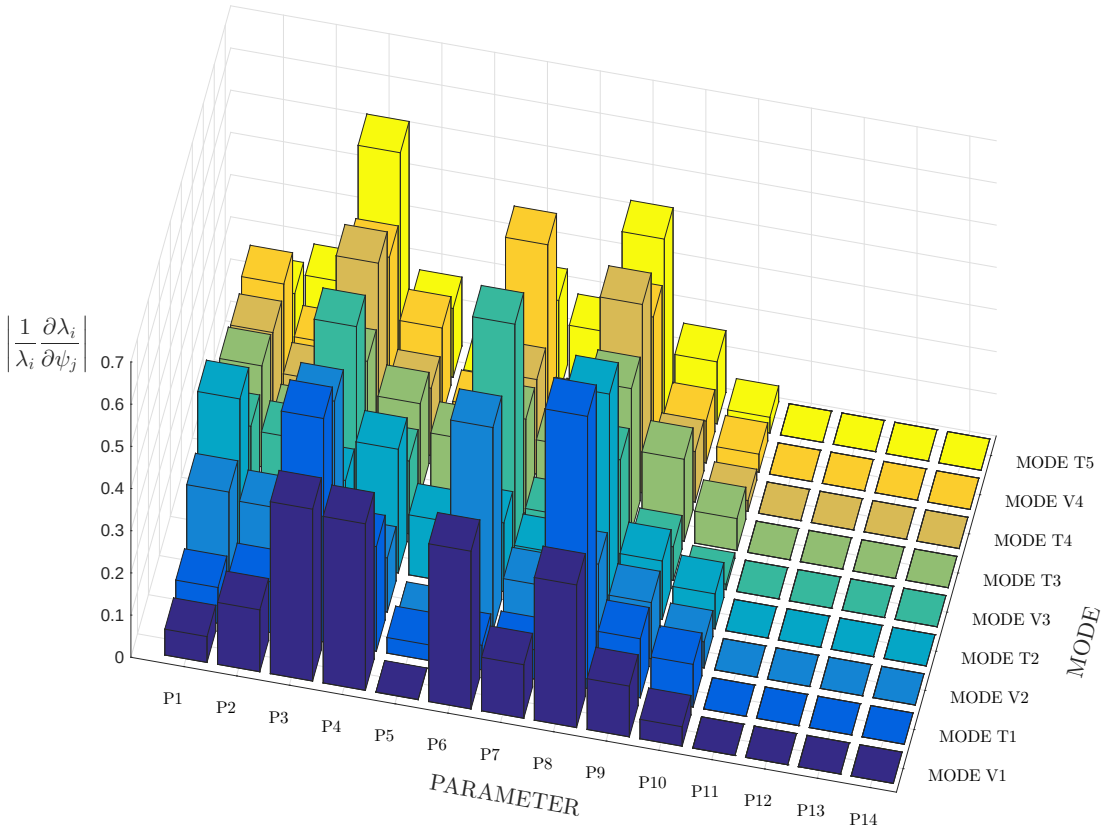

Figure 11: Sensitivity of the eigenvalues of the FEM model on Young's moduli, mass densities and spring coefficients.

The normalized relative sensitivities show that most of the chosen parameters really affect the modal response of the structure. In particular, the plots show that: (i) the parameters that most influence the overall variation of the frequencies are the Young's modulus of the arches (P3), with normalized sensitivity coefficients of six modes over 0.4, and the concrete mass density of the arches (P8), with sensitivities higher than 0.3 for almost all the considered frequencies; (ii) concerning the concrete mass density of the deck (P6), it affects about all the frequencies, with normalized sensitivity coefficients of four modes over 0.3; (iii) the Young's modulus of the deck (P1) is mostly effective on the fourth mode, while the other modes are less influenced; (iv) the elastic modulus of the hangers (P4) essentially influences the frequency of the first mode; (v) the Young's modulus and the mass density of the main longitudinal girders, (P2) and (P7) respectively, the Young's modulus of the upper transverse beams (P5) and the mass density of the hangers (P9) slightly influence about all the modes; moreover, the sensitivities on these parameters are higher than those referred to the mass density of the upper transverse beams (P10); (vi) very small sensitivities are associated to the stiffness coefficients of the springs, despite for the wide assumed range of four orders of magnitude. It shall mean that the latter may display a marginal effect on the frequencies of the bridge, within the present analysis. Despite, additional refined trails may be considered for other values of the spring coefficients apt to set any possible influence on the updating process. This is not here further inspected, while focus is then placed on the intrinsic structural parameters, also considering that a single bridge span has been modelled. Further analyses on the effects of the boundary conditions may be assessed in future investigations.

In light of the obtained results, the first 9 structural parameters (5 Young's moduli and 4 mass densities) listed in Table 2 have been finally selected to be varying during the updating procedure. The outcomes from the automated updating procedure are discussed in following Section 4.2.

In order to test the efficiency of the implemented SA-based LHS method, a SA has also been assessed just on the initiation point representing the parameters of the FEM base model. Hence, variations of the normalized sensitivity coefficients S between those determined through this latter

procedure (hereinafter S^{bm}) and those determined implementing LHS (hereinafter S^{LHS}) have been inquired. As expected, consistent variations have been recorded. In particular, percentage discrepancies $\Delta S = (S^{\mathrm{bm}} - S^{\mathrm{LHS}})/S^{\mathrm{LHS}}$ have resulted to exceed 10% for Mode 1, Mode 5 and Mode 8, by referencing to the Young's modulus of the upper truss beams (P3) (for Mode 8, ΔS has resulted in the order of 45%); for Mode 8, ΔS has also turned out to exceed 10%, by referencing to the Young's modulus of the arches (P3), and to the mass densities of the arches (P8), the hangers (P9) and the upper truss beams (P10), reaching the value of about 63% for the latter. It should be noted that S^{bm} values would have still led to consider in the updating procedure of the Brivio bridge the same parameters selected after the SA-based LHS implementation, namely selected on the basis of values S^{LHS}. This may however be considered as strictly related to the present case study and thus it should not overshadow the consistent percentage discrepancies resulted from the comparison between a one-point-evaluated SA and a complete SA-based LHS.

4.2 FEM model calibration

The procedure for updating the FEM model of Brivio bridge has been conducted involving 200 initiation points, as described in Section 2.2. The number of start points has been chosen as being high enough to obtain a quite dense partitioning of solution domain $D \subseteq \mathbb{R}^9$ (Sections 2.1 and 4.1). Maximum interval d_{max} between two close points along each dimension of domain D is reported in Table 4. Recall that the generation of the initiation point by LHS is fully automated (Section 2.1).

Table 4: Structural properties of the FEM base model (Ref. value) and maximum point distance d_{max} in solution domain D obtained after LHS application, along each space dimension.

No.	Parameter	Symbol	Ref. value	$\mathbf{d_{max}}$	Units
P1	Deck elastic modulus	E_d	34.9	0.206	GPa
P2	Main longitudinal girders elastic modulus	E_{lg}	34.9	0.197	GPa
P3	Parabolic arches elastic modulus	E_a	35.7	0.210	GPa
P4	Hangers elastic modulus	E_h	35.7	0.203	GPa
P5	Upper transverse beams elastic modulus	E_{ub}	35.7	0.207	GPa
P6	Deck mass density	ρ_d	2.44	0.014	t/m^3
P7	Main longitudinal girders mass density	ρ_{lg}	2.44	0.014	t/m^3
P8	Parabolic arches mass density	ρ_a	2.44	0.014	t/m^3
P9	Hangers mass density	ρ_h	2.44	0.014	t/m^3

Before proceeding with the optimization procedure, the FEM model calibration of the bridge has been attempted without involving the global optimization-based LHS, namely by means of a local TR optimization routine, starting from the FEM base model as the only reference initiation point. This conceptually traces what has been done for SA at the end of Section 4.1.1. Results from this preliminary checking are reported in Tables 5–6. Therein, it is possible to note that such results have turned out unsatisfactory, signaling a frequency discrepancy $\Delta f^{\mathrm{FEM}} = (f^{\mathrm{FEM}} - f^{FDD})/f^{FDD}$ to range between 2% and 8% (over 6% for four out of eight modal frequencies), thus endorsing the need for a consistent implementation of a global optimization procedure based on different automatically selected initiation points, specifically conceived and tuned on the refinement of the eigenfrequency estimations (MAC values appear rather satisfactory, except for Mode 7, i.e. T4). Characteristic parameters are varied, most of them by two-digit percentages above 10%, with maximum deviations in the order of 15%.

4.2.1 Algorithmic and computational aspects

As a matter of fact, the parameters describing the characteristic mechanical properties of a structure may be considered to be independent from each other; initiation points characterized by parameters which are actually to be proportionally incremented (or reduced) may therefore be considered as representative of unrealistic situations, within a structural context. In particular, this easily holds true for cases corresponding to the maximum (or minimum) values for all the parameters in the considered ranges, i.e. when the initiation points are located on the edges of the parametric (solution) domain. In light of the evidence that the closer to the authentic optimum solution one may place the initiation point, the higher the recorded probability not to fall on a

Table 5: Comparison between the structural properties of the FEM model before updating (Ref. value) and after updating (Updated value) by means of a local TR optimization routine (i.e. without involving the global optimization-based LHS).

No.	Parameter	Symbol	Ref. value	Updated value	Δ_{par} [%]	Units
P1	Deck elastic modulus	E_d	34.9	39.5	13.27	GPa
P2	Main longitudinal girders elastic modulus	E_{lg}	34.9	40.3	15.46	GPa
P3	Parabolic arches elastic modulus	E_a	35.7	31.8	−11.01	GPa
P4	Hangers elastic modulus	E_h	35.7	38.4	7.68	GPa
P5	Upper transverse beams elastic modulus	E_{ub}	35.7	30.6	−14.16	GPa
P6	Deck mass density	ρ_d	2.44	2.36	−3.34	t/m^3
P7	Main longitudinal girders mass density	ρ_{lg}	2.44	2.73	12.00	t/m^3
P8	Parabolic arches mass density	ρ_a	2.44	2.26	−7.21	t/m^3
P9	Hangers mass density	ρ_h	2.44	2.80	14.85	t/m^3

Table 6: Comparison between experimental (identified) and numerical modal characteristics of the FEM model updated by means of a local TR optimization routine (i.e. without involving the global optimization-based LHS).

Mode	Description	Identified freq. (FDD) [Hz]	FEM freq. [Hz]	Δf^{FEM} [%]	Mutual MAC
V1	1^{st} bending	3.564	3.820	7.19	0.9986
T1	*1^{st} torsion*	*3.857*	*4.046*	*4.90*	*0.0423*
V2	2^{nd} bending	6.018	5.918	−1.67	0.9932
T2	2^{nd} torsion	7.178	6.638	−7.52	0.9913
V3	3^{rd} bending	7.690	7.935	3.19	0.9942
T3	3^{rd} torsion	9.009	8.836	−1.92	0.9374
T4	4^{th} torsion	11.38	10.70	−6.02	0.6862
V4	4^{th} bending	13.09	12.59	−3.83	0.9861
T5	5^{th} torsion	17.02	15.68	−7.88	0.9634

local minimum, points located very close to the edges of the parametric domain should not be really considered in the procedure for updating the FEM model of the structure, since they are unlikely to become close to a potential (local) optimum (see discussion in the Introduction with reference to this subject). Thanks to being based on the criterion of the so-called Latin Square rule (see Section 2.1), the LHS strategy, herein adopted as a way to properly select the initiation points of the updating procedure, automatically considers this aspect. Fig. 12 graphically inspects and returns the evidence of this allegation.

In the plot illustrated in Fig. 12, the horizontal axis depicts the reference number of each Start Point (SP) automatically defined by the LHS procedure, which is an indicator of the corresponding following optimization path; the left vertical axis reports the SP normalized distance in solution domain D, from the point representing the parameters of the FEM base model of the bridge, hereinafter called *Base Point (BP)*. Such a distance is calculated to be equal to Euclidean norm $d = \sqrt{\sum d_i^2}$, where d_i is the non-dimensional point distance along each space dimension, defined as $d_i = (\text{par}_i - \text{par}_i^{BP})/\text{par}_i^{BP}$, where par_i indicates the value of parameter i associated to a specific SP, and par_i^{BP} indicates the value of parameter i referred to the BP (namely the *Ref. value* in Table 2). Moreover, the right axis also represents the distance in term of percentage of the wideness of the solution domain, ranging here from 0.70 to 1.30 of the reference parameter on each space dimension. From Fig. 12 it is possible to note that there appear no points located on the upper part of the plot; this means that the LHS implementation *automatically controls the distribution of the initiation points*, so that they do not get close to the edges of solution domain D, being all included on a hyper-sphere of a radius d at about 0.7, i.e. nearly 25% of the wideness of the parametric space. This holds true also in controlling that SPs do not get too close to the BP, to explore ranges of updating parameters that may drill positions of the parametric space somehow diverging from the BP, in seeking for a possible improvement of the model. Indeed, Fig. 12 depicts that there appear no points located on the bottom part of the plot as well, about below 0.3. Still in light of the above-mentioned evidence referred to the relation between SP and Local Minimum (LM), this

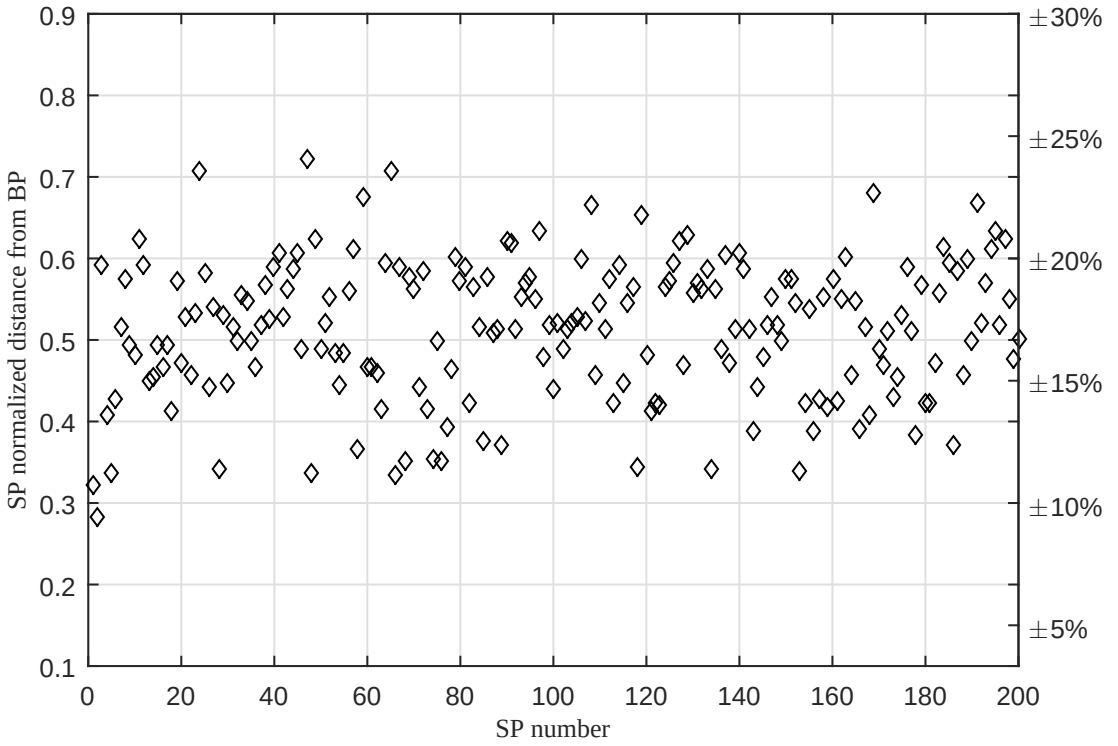

Figure 12: Start Point (SP) normalized distance from Base Point (BP) (left axis) and percentage wideness distance of solution domain (right axis) for each SP.

conceptually means that also cases that might lead to a final (updated) FEM model very similar to the base one are reported as to be unprivileged.

In other words, it is possible to state that the present LHS implementation acts like ad-hoc constraints imposed onto the solution domain of the optimization problem, without any demanding additional computational strategy, in this way providing benefits in terms of computational efforts devoted to the whole FEM model updating procedure.

As stated above in Section 2.2, global minimum $\bar{\boldsymbol{\theta}}^*$ has been selected among set of solutions E as the point characterized by the least (minimum) between the worst (maximum) errors on the frequencies over all the local minima recorded along the different optimization paths started from the various initiation points. Such type of judgment is related to the higher reliability and precision of the frequency data retrieved from the identification process, with respect to the components of the mode shapes, and to the specific goal of refining the frequency estimations by the updated model. Hypothetically, such an assertion would be taken into account by appropriately modifying weighting coefficients α_m in Eq. (3), namely by shifting the importance of the updating information on the frequencies. However, runs conducted operating in that way returned rather unsatisfactory results, thus leading to consider as really necessary also the information coming from the M mode shapes, as a whole, and actually as equally weighted with that from the frequencies toward the identification process ($\alpha_m = 1/(2\mathrm{M})$). This has lead to produce rather reasonable and convenient results, as reported in the following.

Fig. 13 further provides a representative description of the adopted selection criterion (Section 2.2.1) for locating global minimum $\bar{\boldsymbol{\theta}}^*$, among all local optima $\boldsymbol{\theta}^*$. In the plot represented in Fig. 13, the horizontal axis again depicts the reference number of each SP (Fig. 12); the left vertical axis now reports the maximum absolute value of the various entries of frequency residual vector $\mathbf{r}^f$ (see Eq. (4)), calculated at the end of each optimization path; the additional right vertical axis reports a direct reading in terms of the arising absolute percentage error on the estimated frequencies ($\Delta f_m^{\mathrm{FEM}}$, as defined in Section 4.2). Therefore, in Fig. 13 it is possible to identify

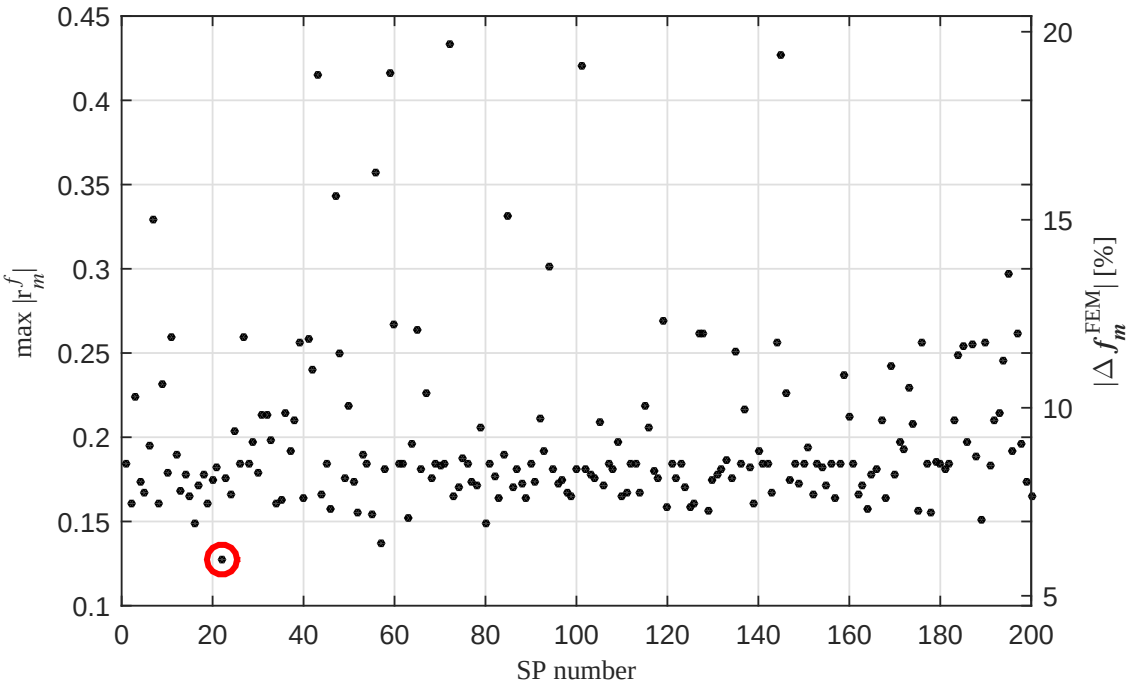

Figure 13: Maximum absolute value of frequency residual vector components r_m^f (see Eq. (4)) and associated maximum absolute percentage error on frequencies $\Delta f_m^{\mathrm{FEM}}$, calculated at the end of each optimization path from each Start Point (SP). Wide red circle identifies the selected global minimum (criterion stated in Section 2.2.1).

the global optimum, among all the local ones obtained from the various (200) LHS automatically-placed start points, as the point displaying the minimum value of maximum residuals $\left|r_m^f\right|$, as well as the minimum value of quantities $\left|\Delta f_m^{\mathrm{FEM}}\right|$. In the plot, the global optimum is marked through a wide circle, as obtained in correspondence of a specific start point, namely SP 22.

Observing Fig. 13, it is possible to appreciate how the (final) local maximum residuals and errors on the frequencies vary through the 200 optimization paths departing from the various LHS-placed SPs, forming the whole optimization procedure. In particular, the major part of the obtained local minima (about 71%) recorded an absolute value of percentage discrepancy $\left|\Delta f_m^{\mathrm{FEM}}\right|$ between 7% and 10%; about 28% of the local minima recorded a $\left|\Delta f_m^{\mathrm{FEM}}\right|$ over 10%; only two local minima recorded a $\left|\Delta f_m^{\mathrm{FEM}}\right|$ lower than 7%. The quite consistent dispersion of the local end points represented in the plot of Fig. 13, surely shows the impending initiation point-localization dependence of the optimization problem and the pertinent outcomes. The contribution of the implemented procedure, in terms of localizing the achieved global optimum, is here demonstrated in overriding this problem. Indeed, the updating methodology has been able to identify a global minimum among all the local ones, despite for their dispersion, really corresponding to an effective model updating of the FEM model of the bridge, starting from a given FEM base model and providing a best improved estimation in the considered range of structural parameters.

This consistent outcome is related to the following considered main aspects, referring to the whole optimization procedure, as key points for the effectiveness of the scheduled model updating LHS implementation in complying with the quest of locating a system realization of the underlying numerical model at best suiting the experimental reality (here in terms of recorded modal properties):

- efficiency of the prodromal implemented SA-based LHS method, in inspecting the sensitivities all around the base point, within the parametric space around it;

- consequent appropriate definition of the main parameters to be involved in the solution domain and of its extension around the base reference;
- further and most important effectiveness of the LHS strategy in automatically defining useful initiation points, un-clustered within the parametric domain, so as to allow for effectively drilling the parametric space and achieving a meaningful global optimization of the whole structural updating process.

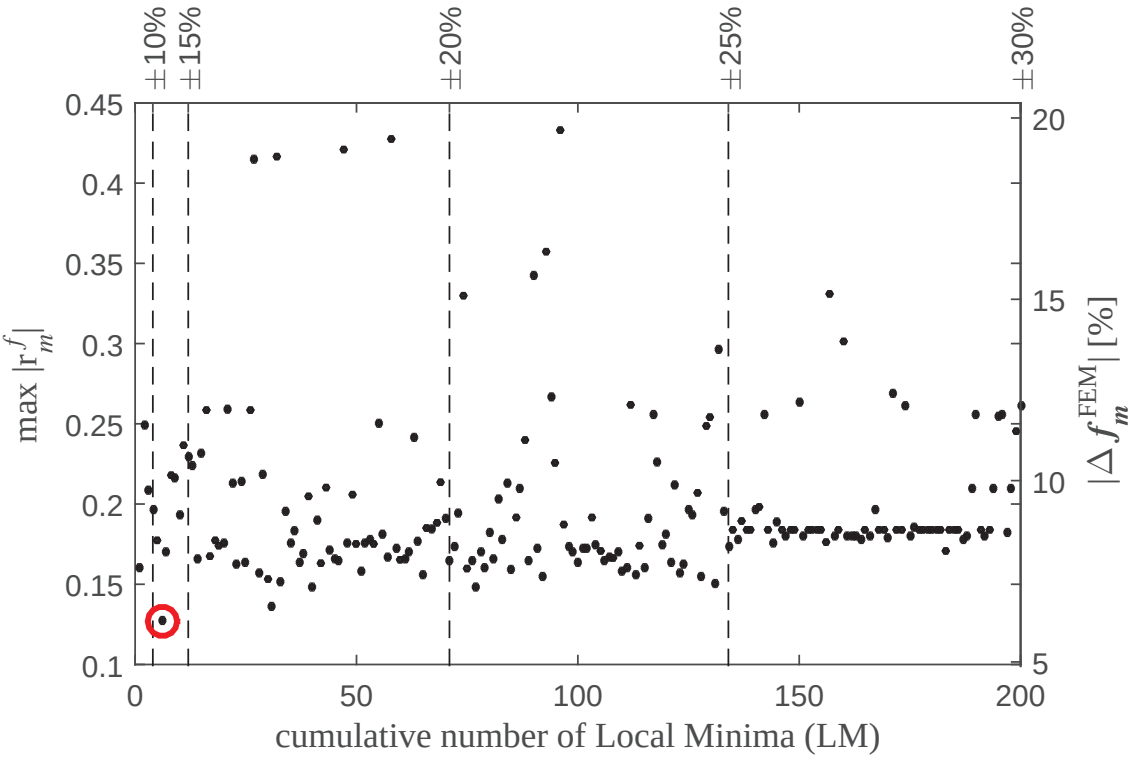

Figure 14: Maximum absolute value of frequency residual vector components r_m^f (see Eq. (4)) and associated maximum absolute percentage error on frequencies $\Delta f_m^{\mathrm{FEM}}$ of the computed Local Minima (LM), ordered according to an increasing range of variation (from 5% to 30%) of the structural parameters obtained after model updating with regard to the initial ones (Ref. value in Tables 5 and 7). Wide red circle identifies the selected global minimum (criterion stated in Section 2.2.1).

Of course, the implemented procedure is also related to the goodness of the starting FEM model of the bridge adopted as *base model*, for the purposes of model updating. In order to appropriately evaluate also this important aspect, Fig. 14 has further been generated for a consistent interpretation and assessment of the obtained updating outcomes. The information thereby reported is complementary to that already provided in Fig. 13. In the plot shown in Fig. 14, on the horizontal axis the plot orders the SPs based on the distance in solution domain D of each Local Minimum (LM) from point BP, i.e. the point representing the parameters of the FEM base model of the bridge; the vertical axes still correspond to those in previous Fig. 13. On the horizontal axis it is thus possible to count the number of LM that have fallen within a determinate distance from BP. From the plot, it is interesting to note that LM that lay in the range $0.75 < d < 0.90$ from BP (corresponding to a variation range of the values of the structural parameters of the base model between ±25% and ±30%) are characterized by an absolute value of percentage discrepancy $\left|\Delta f_m^{\mathrm{FEM}}\right|$ over 8%. This states that LM graved far away from BP do not lead to a considerable improvement of the FEM base model of the bridge. In light of that, the parametric domain of the optimization procedure confirmed itself to be rather appropriate for the pursued model updating finalities.

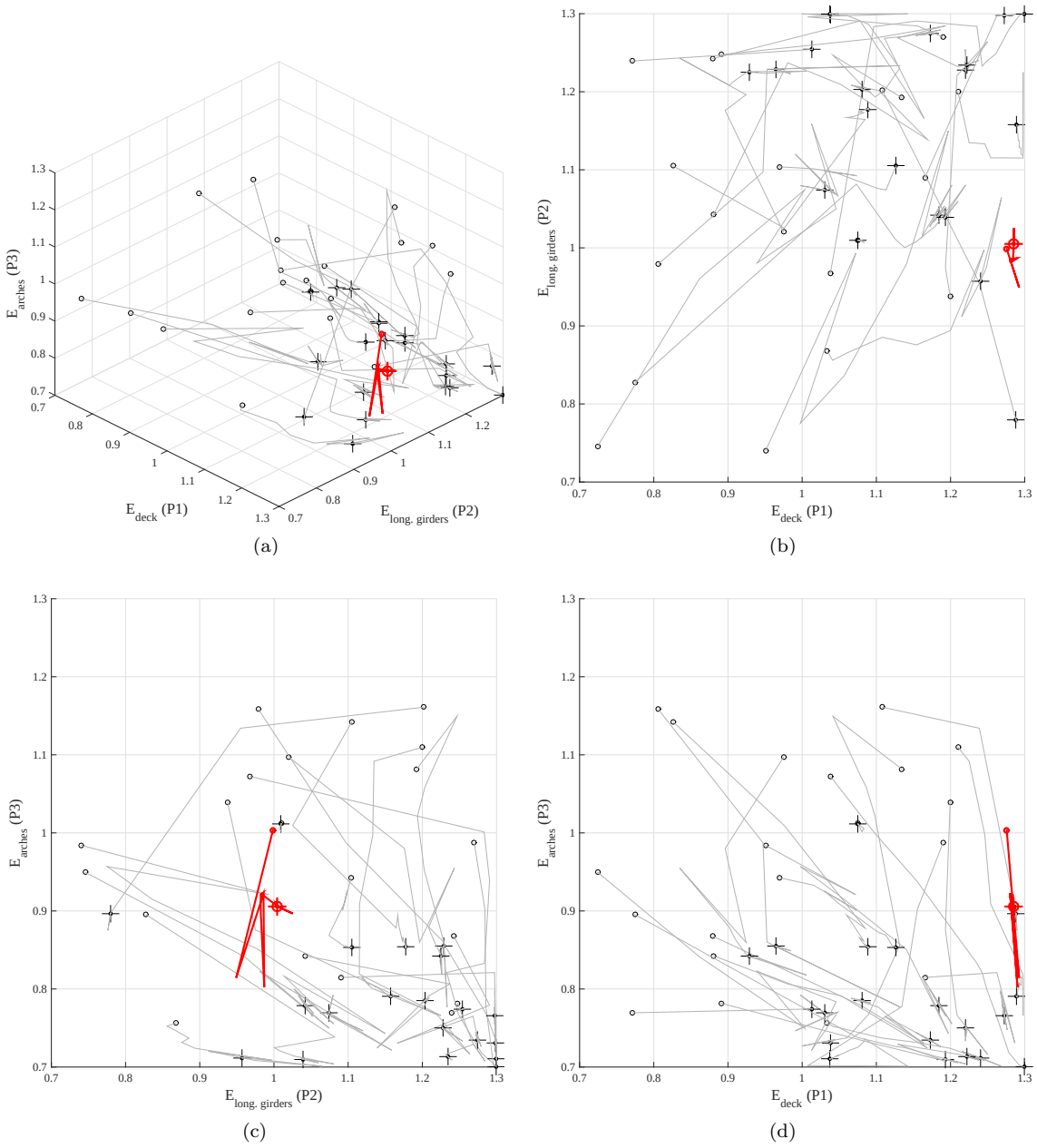

Figure 15: (a) 3D representation and (b)–(d) 2D sections in a 3D sub-domain of parametric domain D, of 20 TR optimization paths (initiation points marked with a small dot and local optimum points marked with a plus sign) and global minimum point (big red circle) obtained by the implementation of the global optimization-based LHS routine.

For a further combined illustration of the LHS-based global optimization process within the parametric space (a 3D subspace of it, referring to the first three elastic moduli to allow for graphical representation, and relevant 2D sections), Fig. 15 also sketches the various optimization paths departing from the automatically selected LHS initiation points and ending up on the corresponding local minima, among whose the global optimum solution is located, according to the criterion stated in Section 2.2.1. The figure allows to appreciate a number of characteristic features of the conceived LHS-based global optimization, such as:

- desired automated and un-clustered distribution of the initiation points;
- distribution of local mimima around the global optimum and their collocation within the parametric space;
- path and distance of each originated local minimum from source LHS-placed initiation point;

- achieved effective filling of the parametric space in seeking the global optimum within a reasonable computational time;
- "spider-net" drilling paths, effectively perforating the parametric space, while clustering and converging toward the zone with the highest attractiveness of local minima, around the global one.

4.2.2 Final updating results

The results obtained from the global optimization-based LHS procedure applied to the FEM base model of Brivio bridge are finally reported in Tables 7–8 and illustrated in Figs. 16–17. In particular: in Table 7 the values of the updated parameters through the optimization procedure are compared with the initial ones; in Table 8 the results of the updating procedure are reported in terms of the final modal frequencies of the structure and of the mutual MAC values, along with discrepancy Δf^{FEM}. Notice that, in Table 8 and in Fig. 16, Mode 2 (T1) is also shown, as it results from the updated FEM model of the bridge, although it was not involved within the updating procedure (Section 4.1).

From the obtained results, it is possible to note that the variation between experimental modal frequencies f^{FDD} and numerical modal frequencies f^{FEM} has been reduced after the updating process. The absolute value of maximum variation Δf has decreased from 9.13% (Table 3) to 6.42% (Table 8). The stated goal of frequency refinement (Section 2.2.1) has been achieved.

The MAC values have been improved as well, all together, for about all of the eight modes of vibration of the bridge considered within the updating process. In particular, MAC values higher than 0.99 have resulted after the updating for four out of the eight considered mode shapes; only for the 7^{th} mode shape (T4) a MAC value less than 0.94 (around 0.7) has been obtained. It is worth to note that such a mode shape is that characterized by the largest complex part (see Fig. 7, Mode 7). The MAC paring matrix between experimental and computed mode shapes of the updated FEM model of the bridge is illustrated in Fig. 17, showing again a rather good correlation, which is quite similar to that already demonstrated in Fig. 10 by the FEM base model.

The values of the parameters of the FEM base model obtained after model updating show that while elastic modulus of the deck E_d and elastic modulus of the main longitudinal girders E_{lg} have been incremented by the optimization procedure, elastic modulus of the parabolic arches E_a and elastic modulus of the upper transverse beams E_{ub} have been reduced (see Table 7); elastic modulus of the hangers E_h has remained more or less unchanged (variation equal to -3.20%), but closer to the elastic modulus of the arches and the upper transverse beams. This shall make sense, since the stiffness of the deck and of the main longitudinal girders of the bridge should in fact be higher than that of the other structural elements, also due to the high ratio of longitudinal reinforcement and a retrofit of the concrete slab carried out in the 1990s. Main recorded variations of the structural parameters are for: E_d, raising by almost 30% to a value of about 45 MPa; E_a, lowering by nearly 10% to about 32 MPa; ρ_{lg}, decreasing by nearly 15% to about 2 t/m^3. Such results would not have been easy to be conjectured by a further manual tuning, without the scheduled automated LHS model updating process.

Table 7: Comparison between the structural properties of the FEM model before updating (Ref. value) and after updating (Updated value).

No.	Parameter	Symbol	Ref. value	Updated value	Δ_{par} [%]	Units
P1	Deck elastic modulus	E_d	34.9	44.8	28.50	GPa
P2	Main longitudinal girders elastic modulus	E_{lg}	34.9	35.1	0.47	GPa
P3	Parabolic arches elastic modulus	E_a	35.7	32.3	−9.41	GPa
P4	Hangers elastic modulus	E_h	35.7	34.6	−3.20	GPa
P5	Upper transverse beams elastic modulus	E_{ub}	35.7	33.7	−5.74	GPa
P6	Deck mass density	ρ_d	2.44	2.43	−0.23	t/m^3
P7	Main longitudinal girders mass density	ρ_{lg}	2.44	2.09	−14.18	t/m^3
P8	Parabolic arches mass density	ρ_a	2.44	2.39	−1.87	t/m^3
P9	Hangers mass density	ρ_h	2.44	2.26	−7.28	t/m^3

Table 8: Comparison between experimental (identified) and final numerical modal characteristics of the updated FEM model.

Mode	Description	Identified freq. (FDD) [Hz]	FEM freq. [Hz]	Δf^{FEM} [%]	Mutual MAC
V1	1^{st} bending	3.564	3.785	6.19	0.9986
T1	*1^{st} torsion*	*3.857*	*4.024*	*4.34*	*0.0422*
V2	2^{nd} bending	6.018	6.021	0.05	0.9909
T2	2^{nd} torsion	7.178	6.769	−5.70	0.9911
V3	3^{rd} bending	7.690	7.958	3.47	0.9921
T3	3^{rd} torsion	9.009	9.165	1.72	0.9436
T4	4^{th} torsion	11.38	10.91	−4.13	0.6814
V4	4^{th} bending	13.09	12.61	−3.68	0.9874
T5	5^{th} torsion	17.02	15.93	−6.42	0.9737

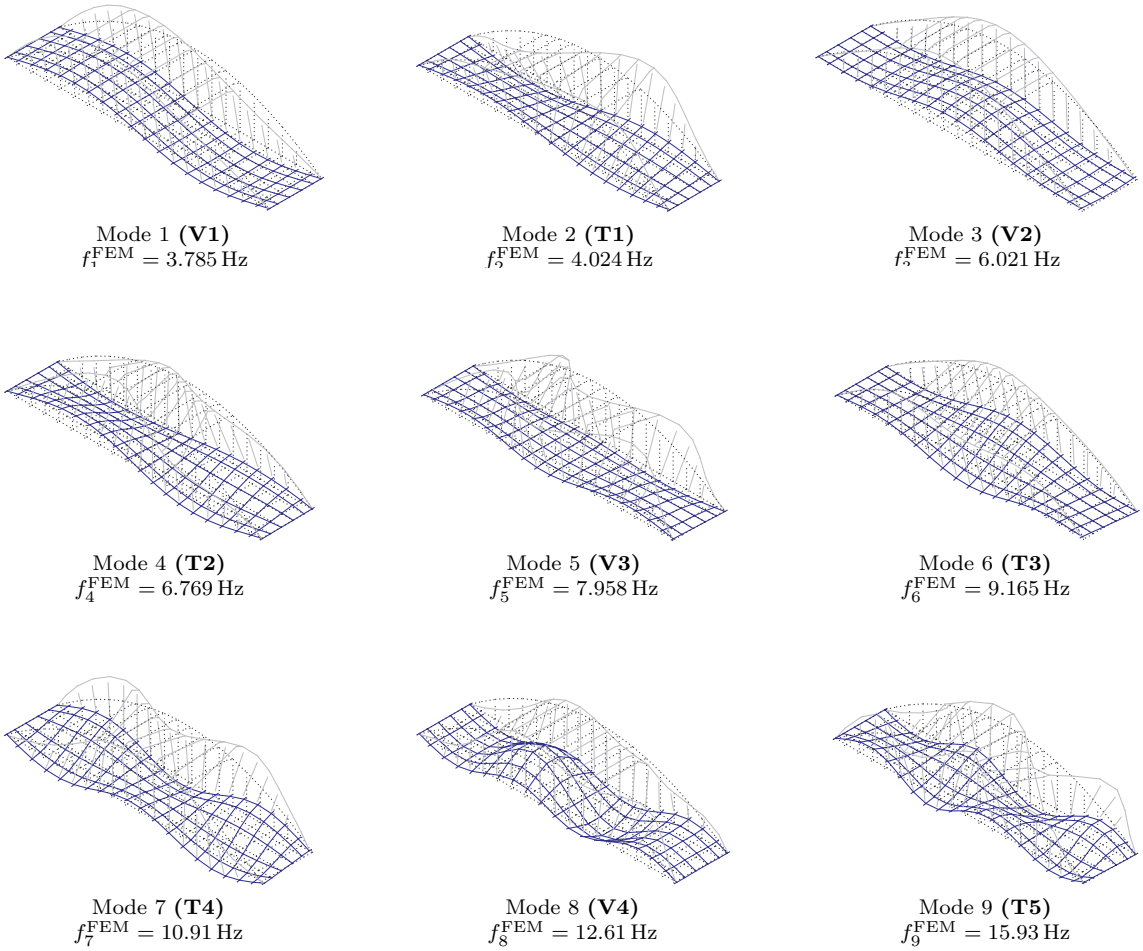

Mode 1 **(V1)** $f_1^{\mathrm{FEM}} = 3.785\,\mathrm{Hz}$

Mode 2 **(T1)** $f_2^{\mathrm{FEM}} = 4.024\,\mathrm{Hz}$

Mode 3 **(V2)** $f_3^{\mathrm{FEM}} = 6.021\,\mathrm{Hz}$

Mode 4 **(T2)** $f_4^{\mathrm{FEM}} = 6.769\,\mathrm{Hz}$

Mode 5 **(V3)** $f_5^{\mathrm{FEM}} = 7.958\,\mathrm{Hz}$

Mode 6 **(T3)** $f_6^{\mathrm{FEM}} = 9.165\,\mathrm{Hz}$

Mode 7 **(T4)** $f_7^{\mathrm{FEM}} = 10.91\,\mathrm{Hz}$

Mode 8 **(V4)** $f_8^{\mathrm{FEM}} = 12.61\,\mathrm{Hz}$

Mode 9 **(T5)** $f_9^{\mathrm{FEM}} = 15.93\,\mathrm{Hz}$

Figure 16: Natural frequencies f_i^{FEM} and mode shapes of the updated FEM model.

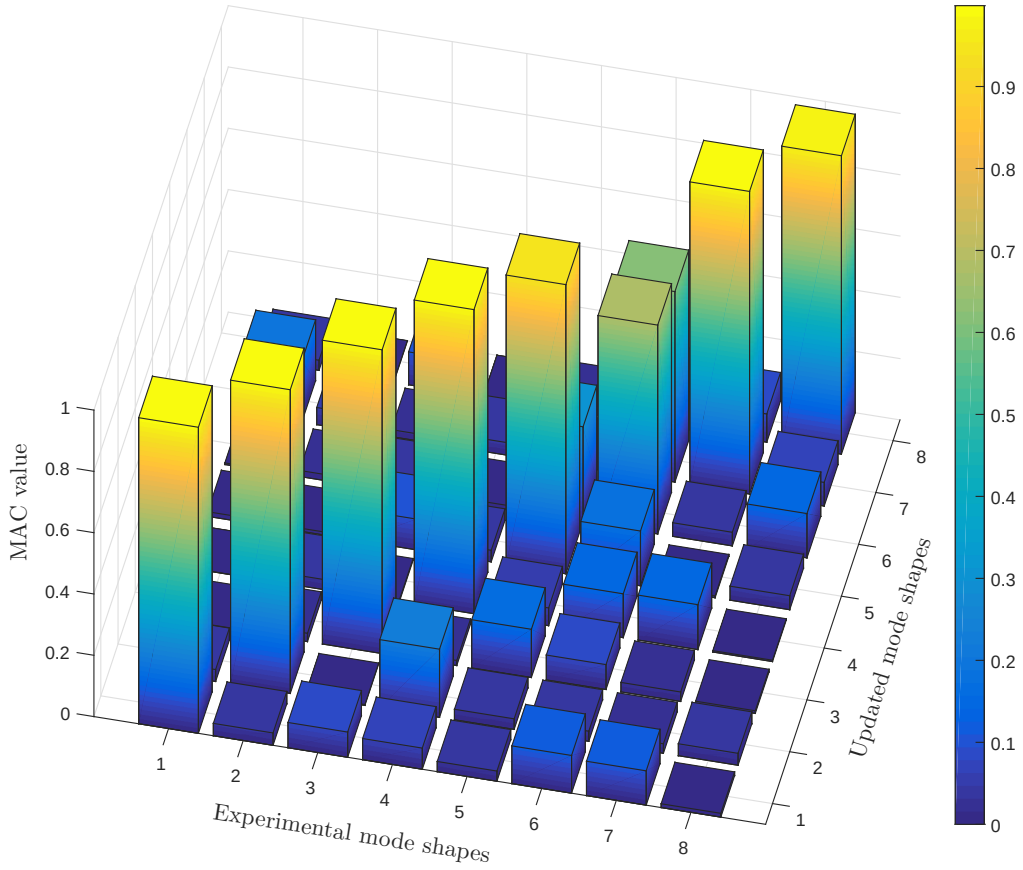

Figure 17: MAC paring matrix between considered eight experimental and computed mode shapes after model updating.

5 Conclusions

In this paper, a Latin Hypercube Sampling, Sensitivity Analysis- and global optimization-based automated model updating self-implementation strategy has been proposed and applied with satisfactory results to a comprehensive case study concerning a FEM model calibration of the historic centennial RC arch bridge at Brivio (1917). Main phases of the outlined case study are summarized in the synoptic scheme of Fig. 18; salient contributions may be itemized in two main points, as detailed in the two subsections below, concerning case study and optimization methodology.

MAIN PHASES OF CASE STUDY ON BRIVIO BRIDGE (1917)

- Experimental campaign with vibrational measurements on spans of the bridge
- OMA modal dynamic identification based on experimental data (FDD + SSI)
- Assembly of linear elastic FEM base model by manual tuning
- LHS Sensitivity Analysis to select structural parameters to be updated
- LHS Global optimization based on modal properties
- Selection of updated parameters and final model-updated FEM model

Figure 18: Synopsis of main phases of case study on FEM model updating of Brivio bridge (1917).

5.1 Case study on Brivio bridge model updating

The advantages of a Sensitivity Analysis and global optimization model updating strategy is fully revealed by the proposed tuning procedure and a challenging model updating of a historic concrete arch bridge is properly achieved. In particular:

- SA is first conducted to locate best-suited structural parameters for the optimization process, among potentially selected ones for the FEM model parametrization. This is obtained through the initiation point-localization independence of SA, automatically implemented via LHS.
- The model updating of centennial Brivio bridge is then efficiently conducted through the implemented global optimization procedure, based on modal properties earlier identified by OMA techniques starting from ambient vibration measurements. The procedure allows for an automated interaction between mechanical FEM solver and numerical optimization loop.
- The structural parameters obtained after model updating are consistent with expected estimates for the the bridge's characteristics. Nine parameters are specifically identified, namely five elastic moduli (ranging from about 32 to 45 GPa) and four densities (varying from nearly 2.1 to 2.4 t/m^3), of the various structural parts, based on information coming from eight modes, in terms of both frequencies and mode shapes, adopted within the model updating process.
- The updating procedure has reduced the discrepancy between experimental and numerical modal frequencies to less than one half of that associated to a manual-tuned FEM base model. Eigenfrequency estimations show consistent values, with contained larger discrepancies in the order of 6%. MAC values on the predicted mode shapes are always consistently derived at around 1, except for a single mode (Mode 7), characterized by coupled bending and torsion, already showing the higher complex components after experimental OMA identification.

Such consistent outcomes make the proposed identification methodology a rather efficient approach for structural updating, in the context of the present case study and likely of similar ones. This shall open up the scene for further investigations of the case study, in which the updated FEM model of the bridge may be adopted for structural analysis purposes, in evaluating both current static and dynamic performances of the structure.

5.2 Methodological approach

A methodological approach has been presented and devised for improving the potential of an optimization procedure relying on a local searching method for finding the global minimum of a specific objective function. In particular:

- The global optimization routine has been set by: (i) requiring several optimization paths to take off from different initiation points, un-clustered and well distributed, so as to fill a user-defined solution domain, and to allow for its effective perforation; (ii) selecting the global minimum among all the (local) minima found at the termination of each optimization path.
- The automated selection of the initiation points is managed by a LHS method, for any located dimensionality of the solution domain and chosen number of start points. The implementation is straightforward and does not require adaptive routines, in association with specific optimization algorithms; it may be adopted for a wide range of optimization problems.
- The LHS method has also been applied at the SA level, thus avoiding the possible initiation point-localization dependence of the resulting optimization problem. Moreover, the evaluation of the derivatives in the SA phase, before starting the optimization process, is performed in full analytical form, allowing to contain the computational burden and to improve performance.

The presented methodology is conceptually simple and readily implementable, while proven successful in the presented challenging case study. It may rely on different local searching methods, other than present Trust Region. Possible additional developments might relate to refined-LHS methods for selecting the initiation points, toward both SA and global optimization processes.

Acknowledgments
The authors wish to thank the Province of Lecco, owner of the Brivio bridge, for granting the permission to perform the experimental tests; the cooperation of MSc A. Valsecchi (Director of the Bridge and Road Division, Province of Lecco) is gratefully acknowledged. The financial support

provided by the University of Bergamo and by ETH Zurich, within project ITALYR (Italian TALented Young Researchers) 2014-2015, and by the Department of Engineering and Applied Sciences (Dalmine) 2015-2016 is also acknowledged.

The Authors wish also to acknowledge public research funding from *"Fondi di Ricerca d'Ateneo ex 60%"* and ministerial doctoral grants and funds at the ISA Doctoral School, University of Bergamo, Department of Engineering and Applied Sciences (Dalmine).

References

[1] Ribeiro D, Calçada R, Delgado R, Brehm M, Zabel V (2012) Finite element model updating of a bowstring-arch railway bridge based on experimental modal parameters. *Engineering Structures* 40:413–435.

[2] Shabbir F, Omenzetter P (2016) Model updating using genetic algorithms with sequential niche technique. *Engineering Structures* 120:166–182.

[3] Bedon C, Dilena M, Morassi A (2016) Ambient vibration testing and structural identification of a cable-stayed bridge. *Meccanica* 51:2777–2796.

[4] Reynders E (2012) System identification methods for (Operational) Modal Analysis: Review and comparison. *Archives of Computational Methods in Engineering* 19(1):51–124.

[5] Friswell MI, Mottershead JE (1995) Finite element model updating in structural dynamics. In: *Solid Mechanics and its Applications, Volume 38*, pp. 263–265.

[6] Mottershead JE, Friswell MI (1993) Model updating in structural dynamics: A survey. *Journal of Sound and Vibration* 167(2):347–375.

[7] Fritzen C-P, Jennewein D, Kiefer T (1998) Damage detection based on model updating methods. *Mechanical Systems and Signal Processing* 12(1):163–186.

[8] Benedettini F, Gentile C (2011) Operational modal testing and FE model tuning of a cable-stayed bridge. *Engineering Structures*, 33:2063–2073.

[9] Ubertini F, Gentile C, Materazzi AL (2013) Automated modal identification and its application to bridges. *Engineering Structures*, 46:264–278.

[10] Pioldi F, Ferrari R, Rizzi E (2016) Output-only modal dynamic identification of frames by a refined FDD algorithm at seismic input and high damping. *Mechanical Systems and Signal Processing*, 68-69(February 2016):265–291, doi: 10.1016/j.ymssp.2015.07.004.

[11] Pioldi F, Ferrari R, Rizzi E (2017) Earthquake structural modal estimates of multi-storey frames by a refined FDD algorithm. *Journal of Vibration and Control*, 23(13):2037–2063, doi:10.1177/1077546315608557.

[12] Pioldi F, Ferrari R, Rizzi E (2017) Seismic FDD modal identification and monitoring of building properties from real strong-motion structural response signals. *Structural Control and Health Monitoring*, First Online: 9 February 2017 (20 pages), doi:10.1002/stc.1982.

[13] Cardoso R, Cury A, Barbosa F (2017) A robust methodology for modal parameters estimation applied to SHM. *Mechanical Systems and Signal Processing* 95(2017):24–41.

[14] Ferrari R, Pioldi F, Rizzi E, Gentile C, Chatzi EN, Klis R, Serantoni E, Wieser A (2015) Heterogeneous sensor fusion for reducing uncertainty in Structural Health Monitoring. In: *UNCECOMP 2015, 1st ECCOMAS Thematic Conference on International Conference on Uncertainty Quantification in Computational Sciences and Engineering*, M. Papadrakakis, V. Papadopoulos, Ed. G. Stefanou, Hersonissos, Crete Island, Greece, May 25-27, 2015, Institute of Structural Analysis and Antiseismic Research, National Technical University of Athens (NTUA), ISBN: 978-960-99994-9-6, pp. 511–528, Eccomas Proceedia ID: 4289, Conference Proceeding ID: 821, doi:10.7712/120215.4289.821, Category: U - MS 1 - INNOVATIVE SENSING SOLUTIONS FOR REDUCING UNCERTAINTY IN ENGINEERING SYSTEMS.

[15] Ferrari R, Pioldi F, Rizzi E, Gentile C, Chatzi EN, Klis R, Serantoni E, Wieser A (2016) Fusion of wireless and non-contact technologies for the dynamic testing of a historic RC bridge. *Measurement Science and Technology* 27(12):124014, doi: 10.1088/0957-0233/27/12/124014.

[16] Ravizza G, Ferrari R, Rizzi E, Chatzi EN (2017) Effective Heterogeneous Data Fusion procedure via Kalman filtering. Submitted for publication, revised version.

[17] Ferrari R, Froio D, Chatzi EN, Gentile C, Pioldi F, Rizzi E (2015) Experimental and numerical investigation for the structural characterization of a historic RC arch bridge. In: *COMPDYN 2015, 5th ECCOMAS Thematic Conference on Computational Methods in Structural Dynamics and Earthquake Engineering*, Eds. M. Papadrakakis, V. Papadopoulos, V. Plevris, Hersonissos, Crete Island, Greece, May 25-27, 2015, Institute of Structural Analysis and Antiseismic Research, National Technical University of Athens (NTUA), ISBN: 978-960-99994-7-2, Vol. 1, pp. 2337–2353, Eccomas Proceedia ID: 3542, Conference Proceeding ID: 1037, doi:10.7712/120115.3542.1037, Category: C - MS 27 - CONDITION ASSESSMENT AND INTERVENTION ON MONUMENTS AND HISTORIC STRUCTURES.

[18] Beck J, Katafygiotis L (1998) Updating models and their uncertainties. I: Bayesian statistical framework. *ASCE Journal of Engineering Mechanics* 124(4):455–461.

[19] Behmanesh I, Moaveni B, Lombaert G, Papadimitriou C (2015) Hierarchical Bayesian model updating for structural identification *Mechanical Systems and Signal Processing* 64-65(2015):360–376.

[20] Bakir PG, Reynders E, De Roeck G (2007) Sensitivity–based finite element model updating using constrained optimization with a trust region algorithm. *Journal of Sound and Vibration* 35:211–225.

[21] Jaishi B, Ren WX (2005) Structural finite element model updating using ambient vibration test results. *Journal of Structural Engineering* 131(4):617–628.

[22] Jaishi B, Ren WX (2006) Damage detection by finite element model updating using modal flexibility residual. *Journal of Sound and Vibration* 290(1):369–387.

[23] Lu Y, Tu Z (2004) A two-level neural network approach for dynamic FE model updating including damping. *Journal of Sound and Vibration* 275(3):931–952.

[24] Moaveni B, Conte JP, Hemez FM (2009) Uncertainty and sensitivity analysis of damage identification results obtained using finite element model updating. *Computer-Aided Civil Infrastructure Engineering* 24(5):320–334.

[25] Nguyen K, Freytag B, Ralbovsky M, Rio O (2015) Assessment of serviceability limit state of vibrations in the UHPFRC-Wild bridge through an updated FEM using vehicle-bridge interaction. *Computers and Structures* 156:29–41.

[26] Polanco NR, May G, Hernandez EM (2016) Finite element model updating of semi-composite bridge decks using operational acceleration measurements. *Engineering Structures* 126:164–277.

[27] Weng S, Xiaa Y, Xua Y-L, Zhub H-P (2011) Substructure based approach to finite element model updating. *Computers and Structures* 89(9-10):772–782.

[28] Jang J, Smyth AW (2017) Model updating of a full-scale FE model with nonlinear constraint equations and sensitivity-based cluster analysis for updating parameters. *Engineering Structures* 83:337–355.

[29] Shan D, Li Q, Khan I, Zhou X (2015) A novel finite element model updating method based on substructure and response surface model. *Engineering Structures* 103:147–156.

[30] Catbas FN, Kijewski-Correa T, Aktan AE (2013) *Structural identification of constructed systems: Approaches, methods, and technologies for effective practice of St-Id*. American Society of Civil Engineers (ASCE).

[31] Guillaume G, Mevel L, Mencik JM, Serra R, Döhler M (2017) Variance analysis for model updating with a finite element based subspace fitting approach. *Mechanical Systems and Signal Processing* 91:142–156.

[32] Boender CGE, Rinnooy Kan AHG (1987) Bayesian stopping rules for multistart global optimization method. *Mathematical Programming* 37(1):59–80.

[33] Suykens JAK, Vandewalle J, De Moor B (2001) Intelligence and cooperative search by coupled local minimizers. *International Journal of Bifurcation Chaos* 11(8):2133–2144.

[34] Jin J (2011) Surrogate-assisted evolutionary computation: recent advances and future challenges. *Swarm and Evolutionary Computation* 1(2):61–70.

[35] Müller J, Shoemaker CA, Piche RA (2013) SO-MI: surrogate model algorithm for computationally expensive nonlinear mixed-Integer, black-box global optimization problems. *Computers and Operations Research* 40(5):1383–1400.

[36] Vincenzi L, Savoia M (2015) Coupling response surface and differential evolution for parameter identification problems. *Computer-Aided Civil and Infrastructure Engineering* 30(5):376–393.

[37] Nocedal J, Wright SJ (1999) *Numerical Optimization*, in: Springer Series in Operations Research. New York: Springer.

[38] McKay MD, Beckman RJ, Conover WJ (1979) Comparison of three methods for selecting values of input variables in the analysis of output from a computer code. *Technometrics* 21(2):239–245.

[39] Saltelli A, Ratto M, Andres T, Campolongo F, Cariboni J, Gatelli D, Saisana M, Tarantola S (2008) *Global Sensitivity Analysis*. The Primer, John Wiley and Sons.

[40] Mottershead JE, Link M, Friswell MI (2011) The sensitivity method in finite element model updating: A tutorial. *Mechanical Systems and Signal Processing* 25(7):2275–2296.

[41] Olsson A, Sandberg G, Dahlblom O (2003) On Latin hypercube sampling for structural reliability analysis. *Structural Safety* 25(1):47–68.

[42] Cavazzuti M (2013) *Optimization Methods: From Theory to Design. Scientific and Technological Aspects in Mechanics*. Heidelberg: Springer. ISBN: 978-3-642-31186-4.

[43] Mokhtar S, Bazaraa MS, Sherali HD, Shetty CM (2006) *Nonlinear Programming*, John Wiley & Sons Inc., Hoboken, New Jersey.

[44] Ferrari R, Cocchetti G, Rizzi E (2016) Limit Analysis of a historical iron arch bridge. Formulation and computational implementation. *Computers and Structures* 175(15 October 2016):184–196, doi: 10.1016/j.compstruc.2016.05.007.

[45] Ferrari R, Cocchetti G, Rizzi E (2017) Computational elastoplastic Limit Analysis of the Paderno d'Adda bridge (Italy, 1889). *Archives of Civil and Mechanical Engineering* 18(1):291–310, doi:10.1016/j.acme.2017.05.002.

[46] Ferrari R, Cocchetti G, Rizzi E (2017) Effective iterative algorithm for the Limit Analysis of truss-frame structures by a kinematic approach. *Computers and Structures* 197(15 February 2018):28–41, doi:10.1016/j.compstruc.2017.11.018.

[47] Simoen E, De Roeck G, Lombaert G (2015) Dealing with uncertainty in model updating for damage assessment: A review. *Mechanical Systems and Signal Processing* 56(2):123–149.

[48] Shahverdi H, Mares C, Wang W, Mottershead J (2009) Clustering of parameter sensitivities: examples from a helicopter airframe model updating exercise. *Shock Vibration* 16(1):75–87.

[49] Friswell MI (1989) The adjustment of structural parameters using a minimum variance estimator. *Mechanical Systems and Signal Processing* 3(2):143–155.

[50] Nelson B (1976) Simplified calculation of eigenvector derivatives. *American Institute of Aeronautics and Astronautics Journal* 14(9):1201–1205.

[51] Brownjohn JMW, Xia PQ, Hao H, Xia Y (2014) Civil structure condition assessment by FE model updating: methodology and case studies. *Finite Elements in Analysis and Design* 37(10):761–775.

[52] Santarella L, Miozzi E (1948) *Ponti Italiani in Cemento Armato*. Milano: Hoepli.

[53] Froio D, Zanchi R (2014) *Finite Element Modelization and Modal Dynamic Analyses of an Historical Reinforced Concrete Bridge with Parabolic Arches*. M.Sc. Thesis in Building Engineering, Advisor E. Rizzi, Co-Advisor R. Ferrari, Università di Bergamo, Scuola di Ingegneria, September 30, 2014, 228 pages.

[54] Brincker R, Zhang L, Andersen P (2001) Modal identification of output-only systems using Frequency Domain Decomposition. *Smart Materials and Structures* 10:441–445.

[55] Peeters B, De Roeck G (1999) Reference-based stochastic subspace identification for output-only modal analysis. *Mechanical Systems and Signal Processing* 13(6):855–878.

[56] Pioldi F, Rizzi E (2018a) Earthquake-induced structural response output-only identification by two different Operational Modal Analysis techniques. *Earthquake Engineering and Structural Dynamics* 47(1):257–264.

[57] Pioldi F, Rizzi E (2018b) Assessment of Frequency versus Time Domain enhanced technique for response-only modal dynamic identification under seismic excitation. *Bulletin of Earthquake Engineering* 16(3):1547–1570.

[58] Zonta D, Modena C (2001) Observation of the appearance of dispersive phenomena in damage structures. *Journal of Sound and Vibration* 241(5):925–933.

[59] Ubertini F, Gentile C, Materazzi AL (2013) Time-frequency analysis of dispersive phenomena in bridges. In: *5th International Operational Modal Analysis Conference (IOMAC 2013)*, Guimarães, Portugal, 2013, 10 pages.

[60] Wang JF, Lin CC (2015) Extracting parameters of TMD and primary structure from the combined system responses. *Smart Structures and Systems* 16(5):937–960.

[61] Salvi J, Rizzi E (2014) Optimum tuning of Tuned Mass Dampers for frame structures under earthquake excitation. *Structural Control and Health Monitoring* 22(4):707–725.

[62] Salvi J, Rizzi E (2017) Optimum earthquake-tuned TMDs: Seismic performance and new design concept of balance of split effective modal masses. *Soil Dynamics and Earthquake Engineering* 110(October 2017):67–80.

[63] Salvi J, Rizzi E, Rustighi E, Ferguson NS (2018) Optimum tuning of passive Tuned Mass Dampers for the mitigation of pulse-like responses. *Journal of Vibration and Acoustics*, ASME, posted online 01 June 2018, Paper No: VIB-18-1027.

[64] Aktan E, Catbas N, Turer A, Zhang Z (1998) Structural identification: analytical aspects. *Journal of Structural Engineering* 124(7):817–829.